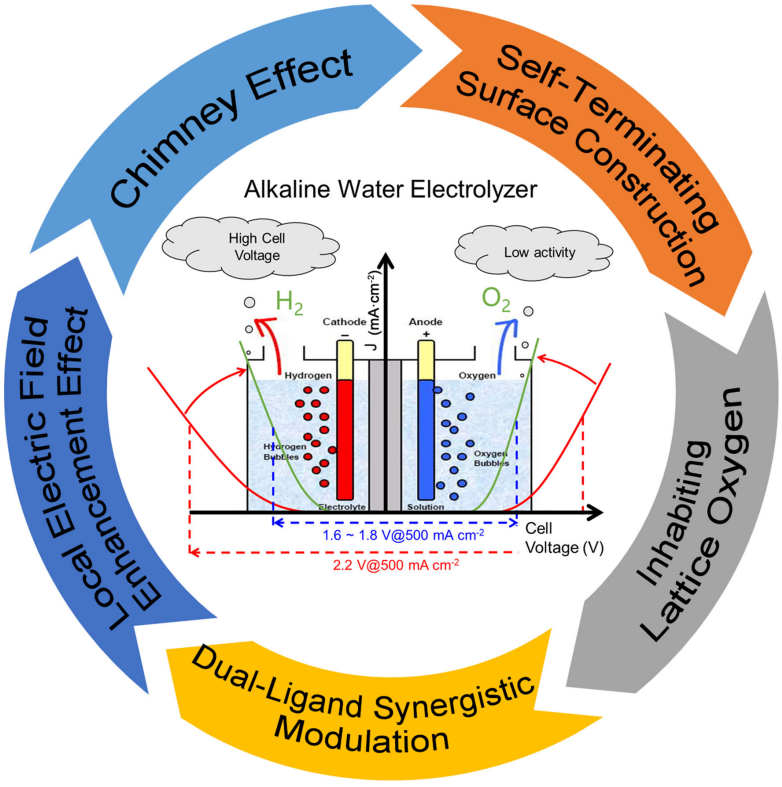
REVIEW

Special Issue on Invited Contributions from Award Winners of the 22nd National Electrochemical Congress in 2024

Series Reports from Professor Wei's Group of Chongqing University: Advancements in Electrochemical Energy Conversions (2/4): Report 2: High-Performance Water Splitting Electrocatalysts

Ling Zhang[a], Wang-Yang Wu[a], Qiu-Yue Hu[a], Shi-Dan Yang[a], Li Li[a,*], Rui-Jin Liao[b], Zi-Dong Wei[a,*]

[a]State Key Laboratory of Advanced Chemical Power Sources (SKL-ACPS), College of Chemistry and Chemical Engineering, Chongqing University, Chongqing, 400044, China
[b]The State Key Laboratory of Power Transmission Equipment & System Security and New Technology, School of Electrical Engineering, Chongqing University, Chongqing 400044, China



Received 30 May 2025; Received in revised form 8 August 2025; Accepted 1 September 2025
Available online 1 September 2025

Li Li and Zi-Dong Wei contributed equally to this work.
*Corresponding author, E-mail: liliracial@cqu.edu.cn (L. Li), zdwei@cqu.edu.cn (Z.-D. Wei).

https://doi.org/10.61558/2993-074X.3583
1006–3471/© 2025 Xiamen University and Chinese Chemical Society. This is an open access article under the CC BY 4.0 license (http://creativecommons.org/licenses/by/4.0/).

Abstract

The unavailability of high-performance and cost-effective electrocatalysts has impeded the large-scale deployment of alkaline water electrolyzers. Professor Zidong Wei's group has focused on resolving critical challenges in industrial alkaline electrolysis, particularly elucidating hydrogen and oxygen evolution reaction (HER/OER) mechanisms while addressing the persistent activity-stability trade-off. This review summarizes their decade-long progress in developing advanced electrodes, analyzing the origins of sluggish alkaline HER kinetics and OER stability limitations. Professor Wei proposes a unifying "12345 Principle" as an optimization framework. For HER electrocatalysts, they have identified that metal/metal oxide interfaces create synergistic "chimney effect" and "local electric field enhancement effect", enhancing selective intermediate adsorption, interfacial water enrichment/reorientation, and mass transport under industrial high-polarization conditions. Regarding OER, innovative strategies, including dual-ligand synergistic modulation, lattice oxygen suppression, and self-repairing surface construction, are demonstrated to balance oxygen species adsorption, optimize spin states, and dynamically reinforce metal-oxygen bonds for concurrent activity-stability enhancement. The review concludes by addressing remaining challenges in long-term industrial durability and suggesting future research priorities.

Keywords: Alkaline water splitting; Hydron evolution reaction; Oxygen evolution reaction; Intrinsic activity; Stability

1. Introduction

Since the Industrial Revolution, the extensive combustion of fossil fuels has powered global development, while triggering severe energy crises and irreversible environmental damage [1–3]. The unsustainable extraction of finite fossil resources now jeopardizes humanity's sustainable future, necessitating urgent transitions to renewable energy alternatives [4–6]. Hydrogen, recognized as an ideal energy carrier due to its natural abundance, high energy density, and zero-carbon footprint, has emerged as a pivotal solution [7, 8]. While conventional hydrogen production relying on fossil fuels poses environmental risks, electrochemical water splitting offers a cleaner pathway. Therefore, integrating renewable electricity from solar, wind, and hydropower enables sustainable green hydrogen generation, marking a transformative shift toward carbon neutrality [9–11].

Water splitting or water electrolysis (WE) can be divided into three categories: alkaline water electrolysis (AWE) [10], proton exchange membrane water electrolysis (PEMWE) [12], and solid oxide electrolysis cells (SOEC) [13]. Currently, AWE is the only commercialized technology owning to its relatively low manufacturing costs. Thermodynamically, the potential of water electrolysis (WE) is 1.23 V, while the cell voltage of industrialized AWE commonly reaches 2.0 V and is even higher [14]. This mainly arises from the high overpotential associated with the hydrogen evolution reaction (HER) at the cathode and the oxygen evolution reaction (OER) at the anode [15–21]. Therefore, both half-reactions require highly active electrocatalysts to lower the overpotentials and enhance the overall energy conversion efficiency. Some noble metal-based materials (Pt/C for HER and RuO_2 or IrO_2 for OER) have been employed in AWE devices. However, their natural scarcity, high price, and unsatisfactory stability significantly barrier their wide application. Despite the fact that numerous non-noble metals based materials have been attempted as substitutes for OER/HER electrocatalysts, such as transition metallic alloys [22–27], phosphides [28–34], carbides [35–41], nitrides [42–45], and sulfides [46–50], their performance still needs to fulfil the requirements of industrialized AWE. This challenge aligns with the fifth question in the Journal of Electrochemistry's "Top Ten Scientific Questions in Electrochemistry": How to rationally design efficient and long-lasting low/non-platinum electrocatalysts and enable their large-scale production [51]? Therefore, developing highly active, stable, non-precious metal electrocatalysts for AWE represents an urgent research priority.

The Wei's Group at Chongqing University has intensively studied alkaline water-splitting mechanisms and advanced electrode engineering, focusing on overcoming HER/OER challenges in WE for industrial-scale applications. To tackle the slow HER kinetics in alkaline electrolytes caused by water serving as both reactant and solvent, the group has proposed effective strategies to enhance active water's mass transfer, activate water dissociation, and optimize hydrogen adsorption and desorption. In addressing the challenge of the trade-off between OER activity and stability, the group focuses on modulating the bonding states of electrocatalysts, balancing the adsorption strength of multiple intermediates, and suppressing the lattice oxygen participation in OER. These approaches allow for the simultaneous improvement in the activity and stability of the OER electrolysts. The deep understanding of alkaline water electrolysis mechanisms established by the Wei's group provides a comprehensive theoretical basis and technical strategy for achieving large-scale energy conservation and efficiency improvement.

2. The Critical Characteristics of the Water-Splitting Mechanism

Electrochemical water splitting ($H_2O(l) \rightarrow H_2(g) + 1/2O_2(g)$), a reaction involving only one water molecule activation and dual gaseous product generation, appears deceptively simple in its stoichiometric representation. Researchers have extensively evaluated numerous potential HER/OER catalysts, testing nearly all electrochemically viable elements across the periodic table, except alkali metals, alkaline earth metals, noble gases, and radioactive elements. Various activity-enhancing strategies have been proposed, including nanoscale catalyst engineering, exposing more active sites, lattice oxygen activation, and key intermediate adsorption energy modulation. However, the ideal electrocatalyst configuration with optimal elemental composition, crystal structure, and morphology simultaneously delivers both high activity and long-term stability remains elusive. The complexity mainly arises from the multifaceted nature of the reaction, where the reaction kinetics and stability depend not merely on electrode intrinsic properties but crucially on the dynamic transport processes at electrode/electrolyte interfaces, especially reactant diffusion and bubble evolution [47, 52–59]. These factors are closely linked to gas electrodes' chemical composition, state, structure, physical morphology, and mechanical strength. To systematically address these challenges, the Wei's research group has proposed a "12345 Principle" framework elucidating critical characteristics in water electrolysis (Fig. 1). This conceptual model comprises: 1. The participation of one water molecule in the electrolysis process; 2. The breaking of two O–H bonds; 3. The involvement of a three-phase boundary in catalysis; 4. Four effects can be considered to improve catalytic performance: electronic, geometrical, electric field, and interfacial effects; 5. Five adsorbed species participated (H*, OH*, O*, OOH*, and H_2O).

Firstly, dissociating one water molecule into hydrogen and oxygen gas under an electric field involves breaking two types of O–H bonds, whether in an acidic, a neutral, or an alkaline solution. As summarized in Table 1 regarding currently proposed HER and OER mechanisms (Reactions 2.1–2.7 for HER and 2.8–2.20 for OER), both the HER mechanism (Reactions 2.4) and OER mechanism (Reactions 2.9, 2.11, 2.13, 2.14, 2.18, 2.19) involve O-H bond cleavage. Reaction 2.4 represents the formation of hydrogen adsorbates (H*) on the electrocatalyst surface through water dissociation in alkaline electrolytes, while the latter describes the generation of oxygen-containing intermediates during the OER process. Although these two types of reactions appear mechanistically distinct, they are fundamentally coupled to sustain continuous water electrolysis because the HER exhibits significant pH dependence, with both its reaction pathway and kinetics being strongly influenced by the pH of electrolytes [52]. For example, a 1 $mol \cdot L^{-1}$ or 6 $mol \cdot L^{-1}$ acid electrolyte allows $H^+(aq.)$ to support a maximum capacity of 26.8 Ah or 6 × 26.8 Ah, indicating that without continuous proton replenishment

Table 1. Summary of HER/OER mechanisms

HER mechanism					
	Acid solutions [52, 53, 60]		Alkaline and neural solutions [61–63]		
Electrode reaction	$2H^+(aq.) + 2e^- \rightarrow H_2(g)$;	2.1	$2H_2O(l) + 2e^- \rightarrow H_2(g) + 2OH^-(aq.)$;	2.4	
Volmer	$H^+(aq.) + * + e^- \rightarrow H^*$;	2.2	$H_2O(l) + * + e^- \rightarrow H^* + OH^-(aq.)$;	2.5	
Heyrovsky	$H^* + H^+(aq.) + e^- \rightarrow H_2(g)$;	2.3	$H_2O(l) + H^* + e^- \rightarrow H_2(g) + OH^-(aq.)$;	2.6	
Tafel	$H^* + H^* \rightarrow H_2(g)$				2.7
OER mechanism					
Adsorption Evolution Mechanism (AEM) [11, 64, 65]			Lattice Oxygen Oxidation Mechanism (LOM) [66–68]		Oxide Path Mechanism (OPM) [69–71]
Step1	$OH^-(aq.) + * \rightarrow OH^* + e^-$;	2.8	$(V_o + O^{latt}H^*) + OH^-(aq.) + * \rightarrow (V_o + O^{latt}H^*) + OH^* + e^-$;	2.12	$OH^-(aq.) + 2* \rightarrow OH^* + * + e^-$; 2.16
Step2	$OH^* + OH^-(aq.) \rightarrow O^* + H_2O(l) + e^-$;	2.9	$(V_o + O^{latt}H^*) + OH^* + OH^-(aq.) \rightarrow (V_o + O^{latt}OH^*) + H_2O + e^-$;	2.13	$OH^* + OH^-(aq.) + * \rightarrow 2OH^* + e^-$; 2.17
Step3	$O^* + OH^-(aq.) \rightarrow OOH^* + e^-$;	2.10	$(V_o + O^{latt}OH^*) + OH^-(aq.) \rightarrow O^{latt}O + H_2O + V_o + e^-$;	2.14	$2OH^* + OH^-(aq.) \rightarrow OOH^* + H_2O + * + e^-$; 2.18
Step4	$OOH^* + OH^-(aq.) \rightarrow O_2(g) + H_2O(l) + * + e^-$;	2.11	$V_o + OH^-(aq.) \rightarrow (V_o + O^{latt}H^*) + e^-$;	2.15	$OOH^* + * + OH^-(aq.) \rightarrow O_2(g) + H_2O(l) + 2* + e^-$; 2.19
Electrode reaction	$4OH^-(aq.) \rightarrow 2H_2O(l) + O_2(g) + 4e^-$				2.20

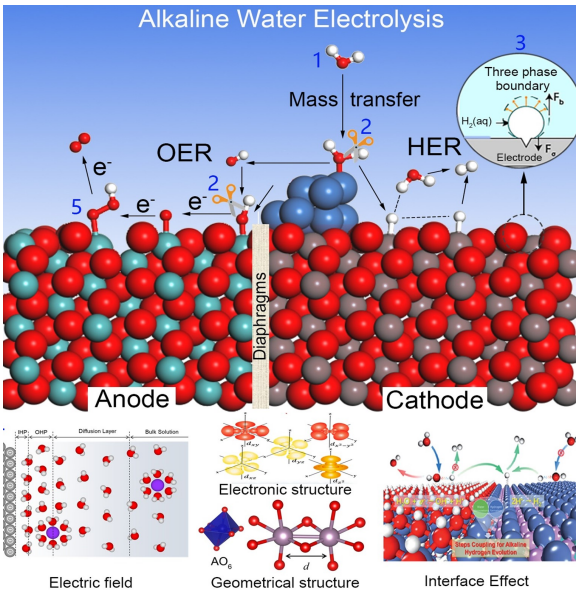


Fig. 1. The "12345 Principle" framework for critical characteristics in water electrolysis.

via O–H bond cleavage in OER, industrial-scale electrolysis at 500 mA·cm^{-2} can only sustain hydrogen evolution for 26.8 hours or 6 × 26.8 hours, correspondingly. Furthermore, continuous H^+(aq.) consumption at the cathode during the HER will progressively increase the electrolyte's pH without timely proton replenishment through the OER. This pH elevation will ultimately alter the rate-determining step of the HER, increase cell voltage, and reduce the hydrogen production rate. Therefore, water electrolysis in both acidic and alkaline electrolytes must overcome the energy barrier of breaking two O–H bonds in water.

Due to the breaking of O–H bonds involving the participation of H^+(aq.), the pH value of the electrolyte affects the reaction kinetics. Mayrhofer et al. discovered that the current density at the same overpotential decreases with increasing electrolyte pH. Moreover, a plateau in the potential range of –0.4 V to –0.9 V (*vs.* SHE) can be observed in the measured polarization curves when the electrolyte's pH value is between 2.5 and 10.5, suggesting that HER activity in this range is controlled by the mass transport of H^+(aq.) rather than charge transfer reactions. When the applied potential is further increased, a steep rise in HER current density can be observed [72]. Undisputed results have also been obtained by Strmcnik's groups [62, 63]. These results demonstrate that water molecules accept electrons to generate hydrogen, contributing to the sharply increasing current density in near-neutral electrolytes when the applied overpotential overcomes the energy barrier of water dissociation. Consequently, water molecules in HER act as both reactants and solvents simultaneously. This dual role can affect water molecule activation, impede proton transfer, and compete with adsorbed hydrogen (H*), and ultimately lead to HER rates in alkaline electrolytes being 2 to 3 orders of magnitude slower than those in acidic solutions.

Secondly, all reactions occur at the three-phase boundaries (TPBs) of the electrode, electrolyte, and gas (solid-liquid-gas interfaces), as both HER and OER involve gas product release. Unlike the stable and continuous solid-liquid interfaces in traditional systems, TPBs are dynamic and intermittent under industrialized conditions in which current densities reach 300 mA·cm^{-2} or higher [29, 55]. These TPBs significantly influence the cell voltage during water electrolysis. Gas products accumulating at TPBs can block ion-conducting pathways, leading to additional energy losses and elevated cell voltages. Furthermore, the massive bubbles generated at the anode and cathode create substantial shear forces that induce local strain, potentially detaching electrocatalysts from conductive substrates and reducing their stability.

Finally, water electrolysis performance can be enhanced through four distinct effects: electronic, geometric, electric field, and interfacial effects. These effects collectively regulate five key intermediates: H*, OH*, O*, OOH*, and H_2O. According to established theories, electrocatalyst activity primarily depends on the adsorption energy of reaction intermediates (ΔE_a, representing adsorbed species), which should ideally exhibit moderate strength (neither too strong nor too weak). However, ΔE_a values for different intermediates are interdependent [65, 73], exhibiting linear scaling relations, competitive adsorption behaviour, or adsorption-desorption trade-offs. A well-known example is the relationship between the adsorption energies of OH* and OOH* during the OER, represented as $\Delta E_{OOH^*} = \Delta E_{OH^*} + 3.1 \pm 0.2$ eV. This scaling leads to a high OER overpotential of about 370 ± 100 mV [66].

Factors such as the equilibrium between H* adsorption and desorption, and the competition between H_2O activation and H* adsorption also play critical roles in the HER. Owning multiple chemical effects, the chemical statement of the electrode is dynamically changed [74]. Precisely regulating the four mechanisms at the three-phase interface of the electrodes under working conditions, optimizing the multidimensional interactions of the five key intermediates, and improving the efficient breaking of the two O-H bonds in the water molecule is essential for promoting the large-scale application of electrolytic water for hydrogen production.

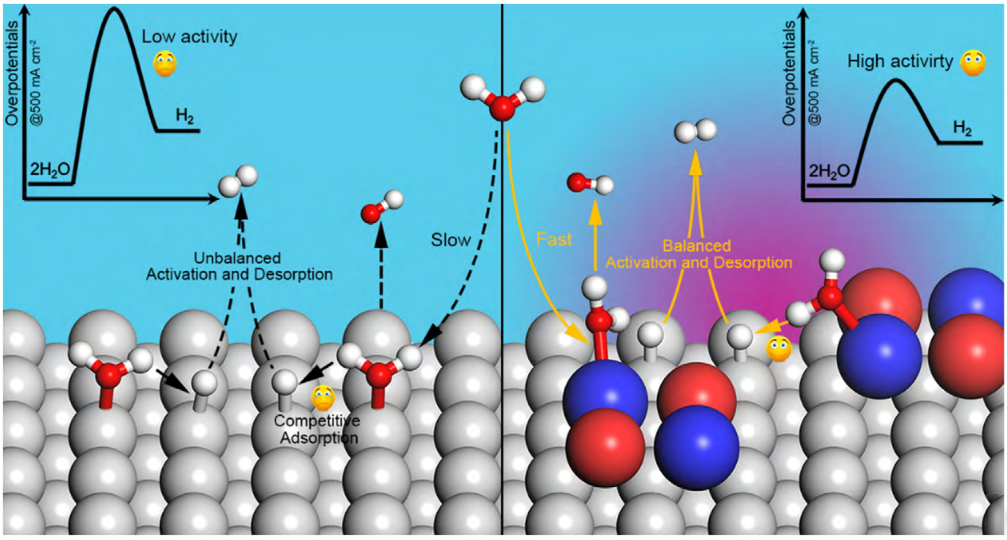


Fig. 2. Scheme illustration of the alkaline HER mechanism and activity enhancement strategies.

3. Alkaline HER Mechanism and Activity Enhancement Strategies

The HER rate in an alkaline solution is 2–3 orders lower than that in an acidic solution, primarily due to water's dual function as both reactant and solvent [61]. The low concentration of protons, unfavourable water dissociation, and competitive adsorption among different intermediates (H_2O, H*, and OH*, as illustrated in Fig. 2) contribute to the slow kinetics of alkaline HER [75–77]. In this case, the active sites of catalysts must balance the H adsorption and H_2 desorption, and facilitate water activation and dissociation. At the same time, the water activation and H adsorption/desorption kinetics should be well matched. Then, constructing hetero-active sites that selectively adsorb H* and H_2O is the key to satisfying the above requirements and enhancing the activity for alkaline HER.

3.1. Chimney effect

Wei's group revealed that charge transfer at the metal/metal oxide interface creates distinct electronic structures, which only selectively adsorbs H* among the three key intermediates, H_2O, OH*, and H* as shown in Table 2, resulting in a "chimney effect" around the metal/metal oxide interface, where H* species are adsorbed, combine into H_2, and then evolute efficiently without the interruption of H_2O and OH* [31, 61]. It significantly enhances HER activity. As shown in Fig. 3a, the interface's unique chemical environment forms a dedicated reaction channel, which benefits H adsorption/desorption, migration, and facilitates rapid H_2 formation and release. Unlike the "spillover effect," which describes the phenomenon of a hydrogen atom migrating from one active site to another due to varying adsorption strengths on the catalyst's surface [76], the "chimney effect"

Table 2. Adsorption energies of H_2O, OH*, and H* on metal/metal oxides

	Adsorption energy / E_{ads} (eV)		
System	H_2O*	OH*	H*
Ni(001)	–0.288	–3.992	–3.983
Bare RuO_2 cluster	–0.781	–3.380	–3.151
RuO_2/Ni(001)			
Ni sites at non-interface	–0.300	–3.961	–3.927
Ni sites at interface	non-absorbable	non-absorbable	–3.687
Ru sites	–0.472	–2.719	–3.852
NiO/Ni(001)			
Ni sites at non-interface	–0.482	–4.487	–3.967
Ni sites at interface	non-absorbable	non-absorbable	–3.592

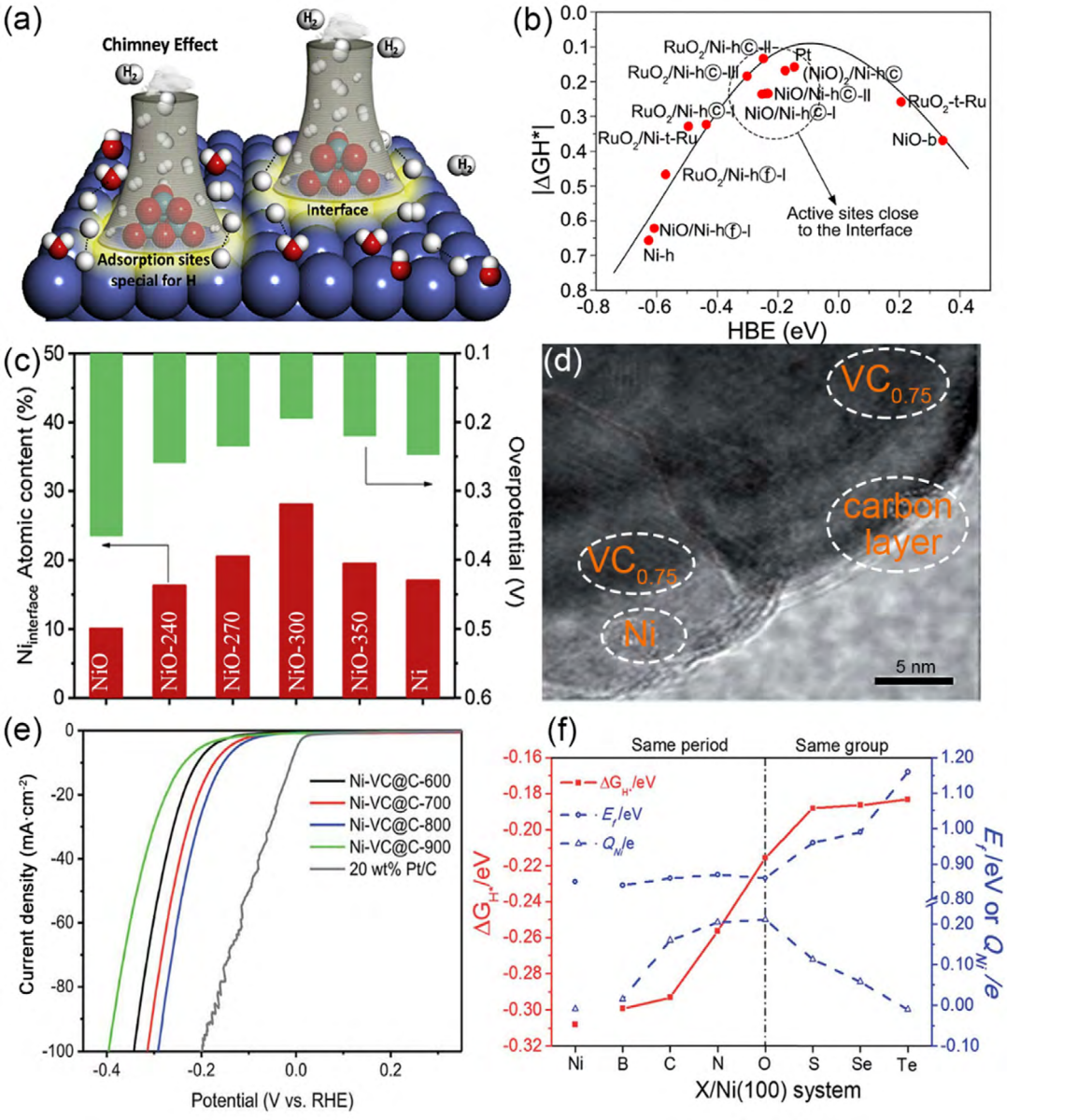


Fig. 3. (a) Schematic diagram of the proposed "chimney effect" on the metal/metal oxide catalysts; (b) Calculated free energy (ΔG_{H^*}) diagram for HER at the equilibrium potential for metal/metal oxides; (c) Comparisons of the number of Ni/NiO interface species on the prepared samples' surfaces and their activities. Reproduced with permission [61]. (d) The transmission electron microscopic (TEM) image of Ni-VC@C/Ti electrode; (e) The linear sweep voltammetric (LSV) curves of Ni-VC@C/Ti electrode and Pt/C in 1 mol·L^{-1} KOH. Reproduced with permission [37]. (f) The H adsorption free energy (ΔG_{H^*}) plots, E_f and Q_{Ni} for each X/Ni(100) system; Reproduced with permission [78].

creates a dedicated reaction channel at the metal/metal oxide interface, which discloses the difference in the adsorption energies of H_2O, OH*, and H* on metal/metal oxides rather than only addresses the behavior of species H* as described by the spillover effect (Fig. 3b, 3c) [61].

The "chimney effect" observed at metal/metal oxide interfaces also exhibits broad applicability to other metal/compound composite catalysts. The modulation strength of HER activity varies depending on the transition metals and nonmetallic elements forming the composite interface. For example, Ni-doped Mo_2C nanowires demonstrated an enhanced HER catalytic activity, achieving a low onset overpotential of 21 mV and requiring only 150 mV to reach 100 mA·cm^{-2}. The Ni and Mo_2C interaction promotes charge redistribution, optimizing the hydrogen adsorption free energy (ΔG_{H^*}) toward thermoneutral values [38]. This modulation strategy is further validated by graphitized carbon-coated Ni-doped vanadium carbide (Ni-VC@C, Fig. 3d, 3e) [37]. Similar enhancements occur with other metal dopants (e.g., Fe in CoP and Mo

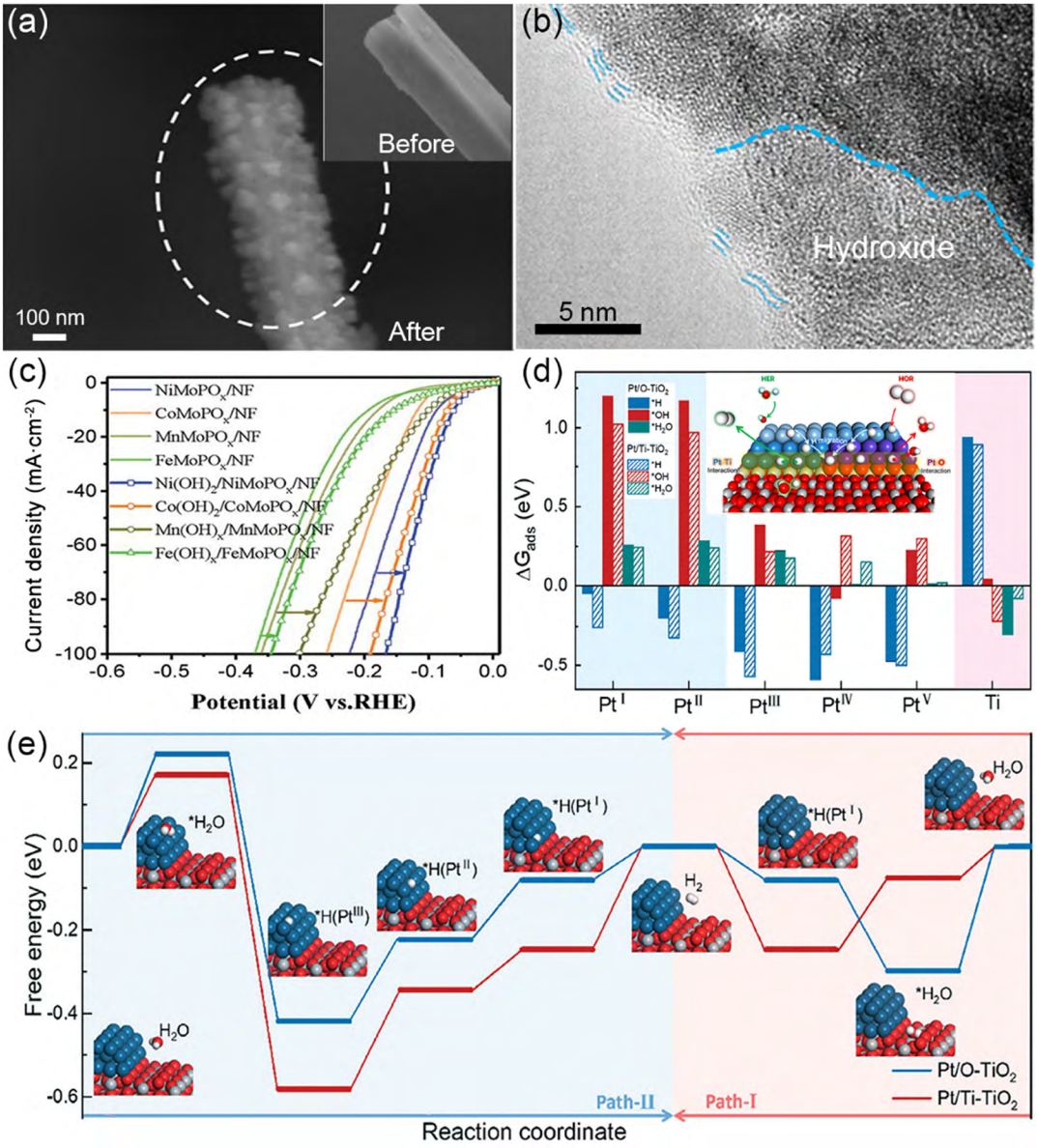


Fig. 4. SEM (a) and TEM (b) images of Ni(OH)$_2$/NiMoPO$_x$ after electrochemical CV activation (Insert: SEM image of Ni(OH)$_2$/NiMoPO$_x$ before CV activation); (c) LSV curves with iR correction for NiMoO$_x$/NF, NiMoPO$_x$/NF, Ni(OH)$_2$/NiMoPO$_x$/NF, 20% Pt/C/NF and NF. Reproduced with permission [31]. (d) Adsorption free energy (ΔG_{ads}) plots of H, OH, and H$_2$O on Pt/O-TiO$_2$ and Pt/Ti-TiO$_2$ (Insert: schematic diagram of Pt/O-TiO$_2$ and Pt/Ti-TiO$_2$); (e) Free energy diagrams of the HER pathway on Pt/O-TiO$_2$ and Pt/Ti-TiO$_2$. Reproduced with permission [81].

in metallic Ni) [26, 79]. For nonmetal doping, Wei's group systematically investigated X/Ni(100) systems (X = B, C, N, O, S, Se, Te; Fig. 3f), identifying electronegativity (χ_X) and principal quantum number (n_X) as key descriptors for predicting HER activity. Notably, VIA-group X atoms (S, Se, Te) significantly boost X/Ni catalytic performance compared to second-period elements, owing to their larger χ_X or n_X values [78].

The "chimney effect" can be further enhanced by increasing interface density, tuning doping elements, and modifying interfacial bonding configurations. As demonstrated in Fig. 4, various composite electrocatalysts, including M-MoPO$_x$ (M = Fe, Co, Ni, Mn) [31], NiO-Ni$_3$S$_2$ [80], and FeO$_x$/Cu$_3$P hydroxide compounds [30], were developed to systematically engineer these interfaces. For the M-MoPO$_x$ system, *in situ* electrochemical CV activation within a specific potential range generated composite interfaces (Fig. 4a, 4b), where different metal elements (Fe, Co, Ni, Mn) modulated the M(OH)$_x$/M-MoPO$_x$ interface properties. Combined theoretical and experimental studies revealed that hydroxide incorporation enhanced water dissociation capability at the M(OH)$_x$/M-MoPO$_x$ interface and optimized

hydrogen adsorption energetics (H*) in the NiMoP catalyst. The resulting $Ni(OH)_2/NiMoPO_x$ catalyst achieved exceptional alkaline HER performance (65 mV@10 $mA{\cdot}cm^{-2}$) and stability, surpassing commercial Pt/C (Fig. 4c) [31]. Similarly, the binder-free FeO_x/Cu_3P@Cu catalyst exhibited outstanding HER activity in 1 $mol{\cdot}L^{-1}$ KOH, requiring only 48 mV overpotential at 10 $mA{\cdot}cm^{-2}$ and outperforming Pt/C at high current densities [30].

The interfacial bonding configuration can also affect the "chimney effect" (Fig. 4d). In Pt/TiO_2 systems, the dominant bonding type dictates distinct catalytic behaviours. When metal-metal (Pt-Ti) bonding prevails at the interface, delocalized electrons induce partial negative charges on interfacial Pt atoms. This electronic environment promotes H migration and water adsorption/activation, thereby accelerating the Volmer step (Fig. 4e). Conversely, interfaces dominated by metal-oxygen (Pt–O) covalent bonding exhibit localized electron transfer, resulting in partially positive Pt atoms. This configuration weakens water adsorption while optimizing H adsorption/desorption, enhances oxidation resistance, and facilitates the Tafel step (Fig. 4e) [81]. This bonding modulation strategy extends to hydrogen oxidation reaction (HOR) catalysts by precisely balancing H and OH adsorption. A representative example is the Ir/MoO_2 catalyst with Ir-O interfacial bonding, where the downshifted d-band centre of surface Ir atoms weakens both H and OH adsorptions. The resulting catalyst achieves exceptional HOR activity (exchange current density: 1.96 $mA{\cdot}cm^{-2}_{ECSA}$), surpassing counterparts with Ir-Mo or mixed interfacial bonding [82].

3.2. Local electric field enhancement effect

Beyond selectively adsorbing key intermediates, the interface can also generate a local electric field enhancement effect. This phenomenon promotes water enrichment and reorientation the adsorption configuration of water molecules at the metal/oxide interface, synergizing with the "chimney effect" to significantly enhance alkaline HER performance (Fig. 5a). Water adsorption configurations are categorized into three types based on hydrogen atom orientation (Fig. 5b): "H-up" (hydrogen away from the electrocatalyst

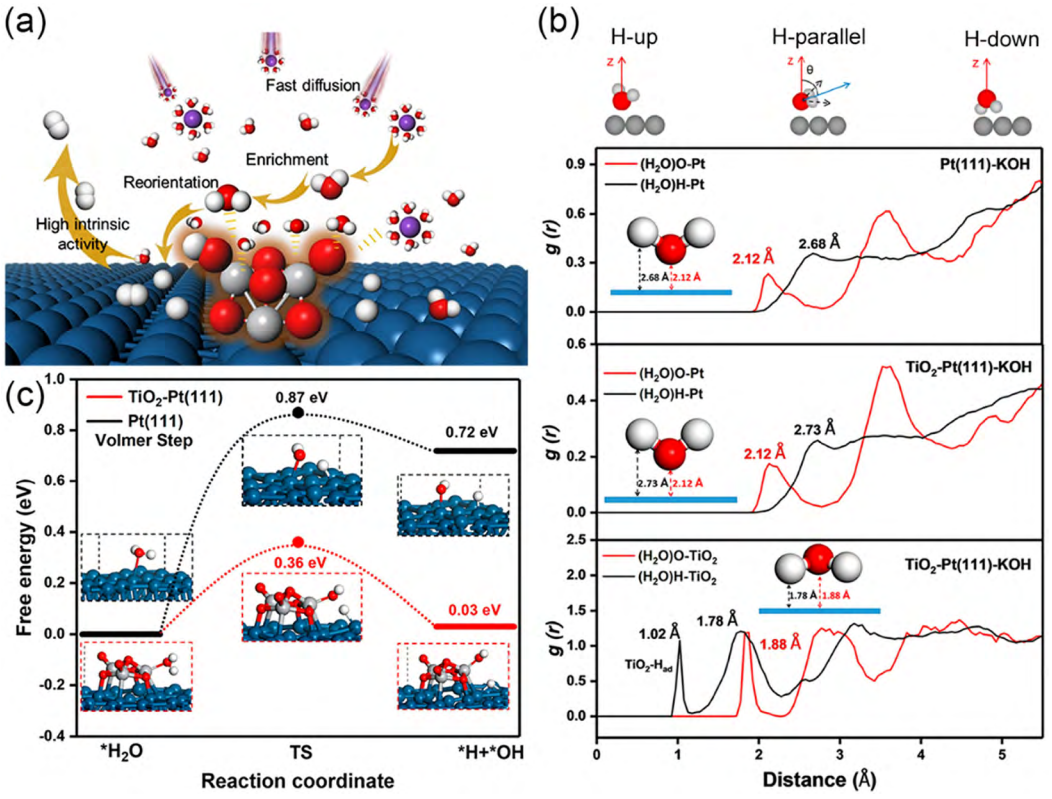


Fig. 5. (a) Illustration of interfacial water enrichment and reorientation on Pt/C catalysts induced by metal oxides participation; (b) Radial distribution function (RDF) of Pt(111)-water and TiO_2-water for Pt(111) and TiO_2-Pt(111) in KOH solution (Top are the schematic illustrations of the three adsorption configurations of water molecules: "H-up", "H-parallel", and "H-down"); (c) The energy barrier plots of water dissociation (Volmer step) on TiO_2-Pt(111) and Pt(111). The illustration shows the corresponding structure. The navy blue, gray, white, and red spheres represent Pt, Ti, H, and O atoms, respectively. Reproduced with permission [75].

surface), "H-down" (hydrogen toward the surface), and "H-parallel" (hydrogen parallel to the surface). Wei's group revealed that the adsorption configurations of interfacial water molecules critically influence HER water dissociation kinetics, which is called the local electric field enhancement effect (Fig. 5a) [75]. This explains why Pt/C catalysts, despite their high intrinsic activity, exhibit slower alkaline HER kinetics under high polarization compared to transition metal catalysts. Unlike transition metal compounds, Pt maintains a metallic character even under strong cathodic polarization. As a result, water molecules primarily adopt two unfavorable adsorption configurations on its surface: "H-up" and "H-parallel" (Fig. 5b). DFT calculations indicate that these configurations impede efficient water activation and dissociation, as shown in Fig. 5c [75].

In contrast, transition metal compounds (oxides or phosphides) retain their oxide surfaces even under high cathodic overpotentials. At these oxide surfaces, interfacial water molecules predominantly adopt an "H-down" orientation, with hydrogen atoms directed toward the catalyst - a configuration that significantly facilitates water activation and dissociation. This explains why numerous studies have observed superior HER kinetics in transition metal compound catalysts compared to Pt/C at high current densities [75].

Guided by these findings, they decorated Pt/C catalysts with hydrophilic metal oxides (MO_x) to create composite interfaces. This strategy combines Pt/C's intrinsic HER activity with enhanced performance at high current densities. The MO_x/Pt interface generates a local electric field that promotes hydrated cation diffusion, enriching active water at the interface (Fig. 6a, 6b). MO_x electrostatically rearranges interfacial water within the compact layer into the "H-down" orientation, facilitating water dissociation (Fig. 6c, 6d). Protons then migrate to the interface, where the "chimney effect" accelerates H_2 formation and desorption. These synergistic effects dramatically improve HER performance under industrial conditions [75]. For instance, TiO_2-CoP composite catalysts lowered the overpotential from 107 mV to 61 mV@ 10 mA·cm^{-2}. Similar improvements were achieved by incorporating small amounts (< 10 at%) of amorphous oxides (WO_3, TiO_2, CeO_2, NiO) into Pt/C catalysts. Notably, TiO_2-Pt/C reduced the overpotential at 500 mA·cm^{-2} from > 400 mV to just 100 mV, demonstrating remarkable kinetic enhancement (Fig. 6e) [77].

Further coupling the "chimney effect" and local electrical field induced by the composite catalysts by modulating the density of the interfacial active sites can effectively strengthen the mass diffusion, interfacial water reorganization, and H_2 evolution to boost HER activity in industrial conditions. Departing from conventional vertically aligned nanoarray fabrication methods, the Wei's group pioneered a novel synthesis of Fe-rich macroporous CoFeP triangular plate arrays (Macroporous CoFeP TPAs/Ni) as high-performance bifunctional water-splitting catalysts. Using CoFe bimetal-organic framework triangular plate arrays (CoFe-MOF TPAs/Ni) as precursors, they selectively etched organic ligands to create interconnected macropores, followed by phosphorization to yield the final catalyst. This structure enhances the local electric field effect, enriching active water and optimizing interfacial water orientation, which, combined with the "chimney effect", dramatically boosts alkaline HER activity. The resulting Macroporous CoFeP TPAs/Ni demonstrated exceptional HER performance, requiring overpotentials of just 43, 113, and 263 mV to achieve current densities of 10, 100, and 900 mA·cm^{-2}, respectively (Fig. 6f) [79]. Morphological control can further create superaerophobic structures to improve bubble release and electrolyte transport. For example, Ni-Co-P hollow prismatic nanoneedle arrays (Ni-Co-P HPONs) were synthesized using NiCo-MOF microprisms as self-sacrificing templates. After urea-assisted hydrothermal transformation, the solid precursors evolved into hollow structures with ordered nanoneedles, enabling outstanding HER activity (205 mV @ 800 mA·cm^{-2}) [54].

4. OER Mechanism and Performance Improvement Strategies

Serving as the anode counterpart to HER, OER faces persistent challenges in balancing catalytic activity with operational stability. Despite decades of research and extensive exploration of diverse materials, few OER electrocatalysts meet the stringent requirements for alkaline water electrolysis (AWE) systems. In stark contrast, advanced HER catalysts already achieve overpotentials below 50 mV at –10 mA·cm^{-2} and even can be less than 10 mV [83–87].

The OER exhibits significantly higher overpotentials (several hundred millivolts) than HER at equivalent current densities while facing persistent stability challenges. Nearly all OER electrocatalysts undergo surface reconstruction to form amorphous hydroxides, activating lattice oxygen that participates in oxygen generation. This irreversible lattice oxygen release structurally destabilizes catalysts, ultimately causing deactivation [68, 88–90]. Critical stability limitations further arise from the dissolutions of active sites across both noble metals (Ru, Ir) and non-noble elements (Fe, Mo, V) [91–96]. Serhiy Cherevko's team demonstrated that even state-of-the-art IrO_2 and RuO_2 could be gradually dissolved in acidic/alkaline electrolytes, with RuO_2 exhibiting faster degradation

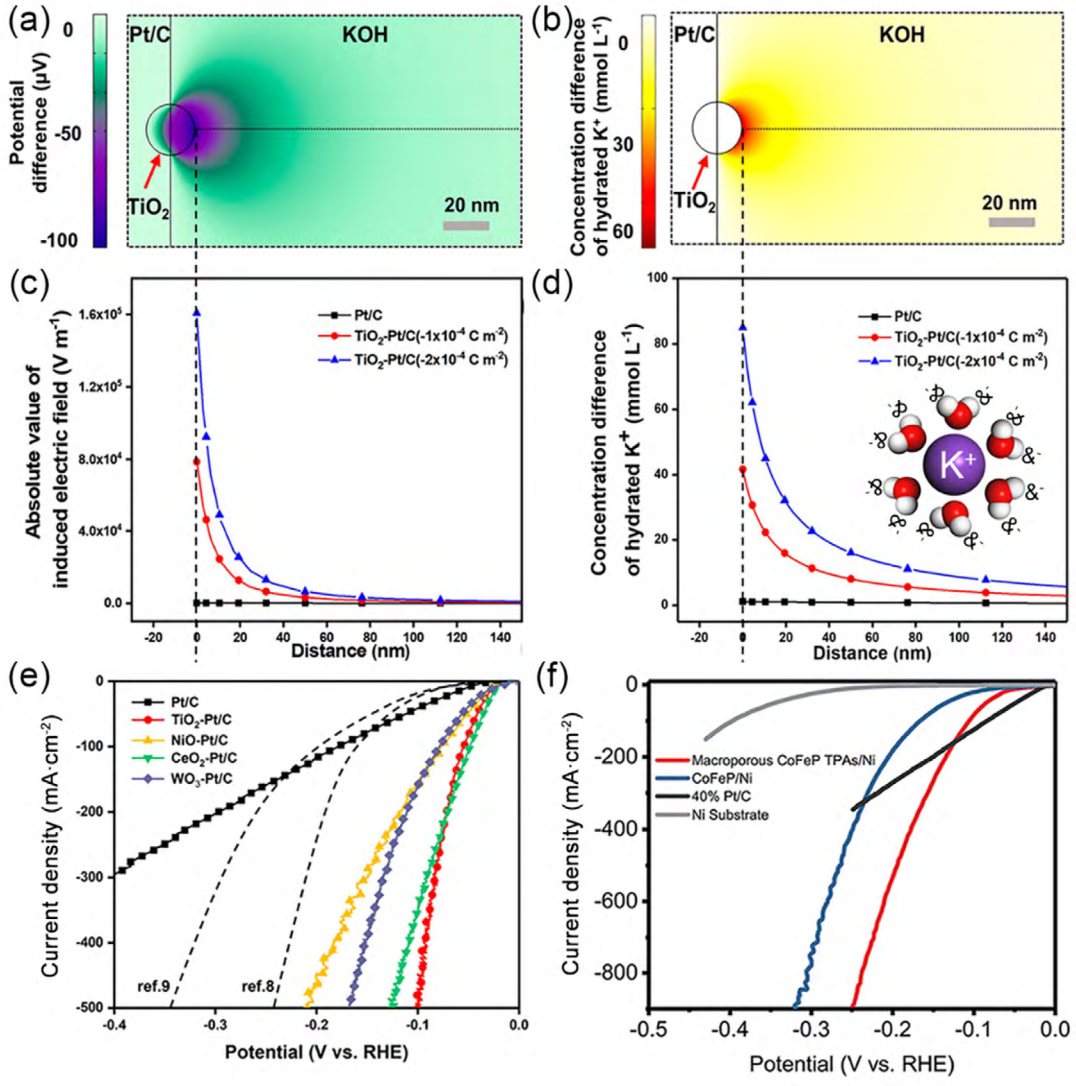


Fig. 6. Simulated distributions of potential (a) and hydrated K^+ concentration (b) by the finite-element method (FEM) for TiO_2-Pt/C at an applied electrode charge density of –1 × 10^{-4} C·m^{-2}; The longitudinal distributions of the absolute value of an induced electric field (c) and hydrated K^+ concentration (d) difference from the electrode surface to solution bulk for TiO_2-Pt/C at applied electrode charge densities of –1 × 10^{-4} C·m^{-2} and –2 × 10^{-4} C·m^{-2}, respectively. Reproduced with permission [75]. (e) LSV curves of Pt/C, TiO_2-Pt/C, NiO-Pt/C, CeO_2-Pt/C, and WO_3-Pt/C. Reproduced with permission [77]. (f) LSV curves of Macroporous CoFeP TPAs/Ni and the benchmark of Pt/C electrocatalysts. Reproduced with permission [79].

than IrO_2 [96]. Similarly, Curtis P. Berlinguette's group revealed Fe dissolution from NiFe-based catalysts at currents below 10 mA·cm^{-2} [92]. These processes alter active sites' chemical states at molecular scales. Therefore, Enhancing OER stability necessitates two critical strategies: controlled managements of surface reconstruction and suppression of lattice oxygen activity, which collectively address structural degradation mechanisms.

4.1. Self-Terminating surface construction

Wei's group discovered that heterointerface engineering can mitigate surface deterioration while balancing lattice oxygen activation and dissociation, as the V_2O_3/CoOOH heterointerface exemplifies. The team developed a highly active Fe/V-doped CoOOH phase for OER through in situ reconstruction of Fe-modified Co_2VO_4 precursors (Fig. 7a) [97]. During reconstruction, partial V leaching accelerates surface restructuring, while residual V forms alkali-resistant V_2O_3 within the CoOOH layer, enabling dynamic charge compensation to prevent excessive lattice oxygen loss and Co dissolution (Fig. 7a). Fe doping promotes Co pre-oxidation and enhances lattice oxygen participation by elevating the O 2p band centre, conferring structural flexibility. The optimized $Co_2Fe_{0.25}V_{0.75}O_4$ electrode achieves exceptional performance, requiring

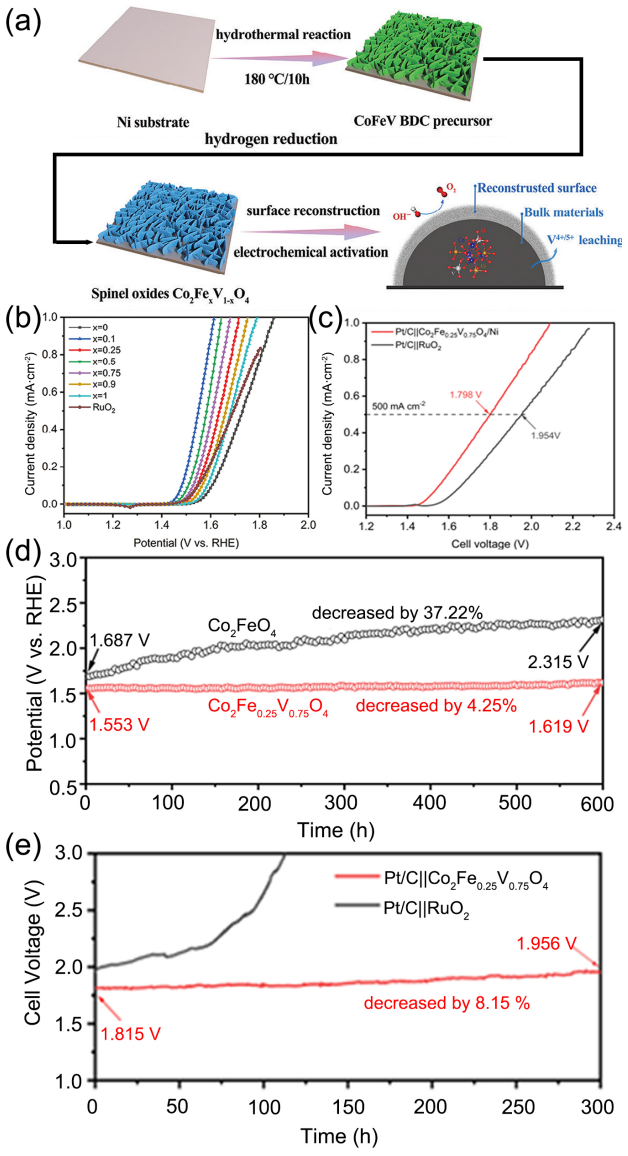


Fig. 7. (a) Schematic illustration for the fabrication of $Co_2Fe_xV_{1-x}O_4$; (b) LSV curves of $Co_2Fe_xV_{1-x}O_4$ (x = 0, 0.1, 0.25, 0.5, 0.75, 0.9, and 1) in O_2-saturated 1 mol·L^{-1} KOH with a scan rate of 2 mV·s^{-1}; (c) Water splitting performance of the Pt/C // $Co_2Fe_{0.25}V_{0.75}O_4$ toward water splitting in 1 mol·L^{-1} KOH; Durability tests under 500 mA·cm^{-2} of $Co_2Fe_{0.25}V_{0.75}O_4$ and Co_2FeO_4 electrodes in the three-electrode system (d) and industrialized electrolyzer (e). Reproduced with permission [97].

overpotentials of merely 205 mV and 320 mV to reach 10 and 500 mA·cm^{-2}, respectively (Fig. 7b). In a practical alkaline electrolyzer ($Co_2Fe_{0.25}V_{0.75}O_4$||Pt/C), a current density of 500 mA·cm^{-2} was sustained at a low cell voltage of 1.798 V, outperforming commercial RuO_2||Pt/C systems (Fig. 7c). Stability tests further demonstrated 600-hour durability in a three-electrode configuration (Fig. 7d) and 300-hour operation in industrial electrolyzers (Fig. 7e) [97].

Building on the advantages of heterointerface engineering, Wei's group developed a coral-like FeNi(OH)$_x$/Ni heterostructure through a combined hydrogen-bubble-assisted deposition and Fe(NO$_3$)$_3$-mediated mild corrosion strategy [98]. The resulting heterointerface features amorphous FeNi(OH)$_x$ shells strongly bonded to crystalline Ni cores, forming a binder-free hierarchical architecture when integrated with an electrodeposited coral-like Ni skeleton and macroporous Ni foam substrate. This unique design simultaneously maximizes active site exposure, enhances mass transport efficiency, facilitates gas bubble release, and improves operational stability [98].

4.2. Inhabiting lattice oxygen

Beyond heterointerface engineering, modulating metal-oxygen (M–O) bond states offers an effective approach to balancing lattice oxygen activation and dissociation, enhancing activity and stability. Wei's group demonstrated this through an interstitial silicon-doping strategy in RuO_2, which suppresses lattice oxygen oxidation while preserving catalytic sites (Fig. 8a) [68]. Band structure analysis reveals that Si doping upshifts the Ru 4d band centre (ε_d) from −1.759 eV to −1.626 eV and downshifts the O 2p band centre (ε_p) from −3.365 eV to −3.850 eV. This can enlarge the gap between the Ru 4d band centre (ε_d) and the O 2p band centre (ε_p), and reduce the covalency of Ru-O in Si-RuO_2. Furthermore, the stronger Si-O bond dissociation energy (798 kJ·mol^{-1} *vs.* Ru-O's 481 kJ·mol^{-1}) enhances lattice oxygen anchoring (Fig. 8b). These dual effects significantly suppress lattice oxygen activation in Si-RuO_x-0.1, as evidenced by differential electrochemical mass spectrometry (DEMS), showing a 95% reduction in lattice oxygen oxidation compared to commercial RuO_2 (Fig. 8c). The optimized Si-RuO_2-0.1 catalyst achieved exceptional performance: a low overpotential of 226 mV at 10 mA·cm^{-2} (Fig. 8d) and minimal degradation (~52 μV·h^{-1}) over 800 hours (Fig. 8e). This strategy uniquely weakens Ru-O covalency without compromising Ru-O structural integrity, providing a blueprint for designing stable OER catalysts [68].

4.3. Dual-Ligand synergistic modulation

A critical challenge in industrial OER catalyst development lies in overcoming the fundamental activity-stability trade-off. Oxygen gas is paramagnetic and can be attracted to ferromagnetic materials like nickel and iron-based OER electrocatalysts. This attraction can block the active sites of the catalysts and reduce their activity [99]. Wei's group addressed this limitation through an innovative dual-ligand synergistic modulation strategy, which concurrently enhances activity and stability (Fig. 9a)

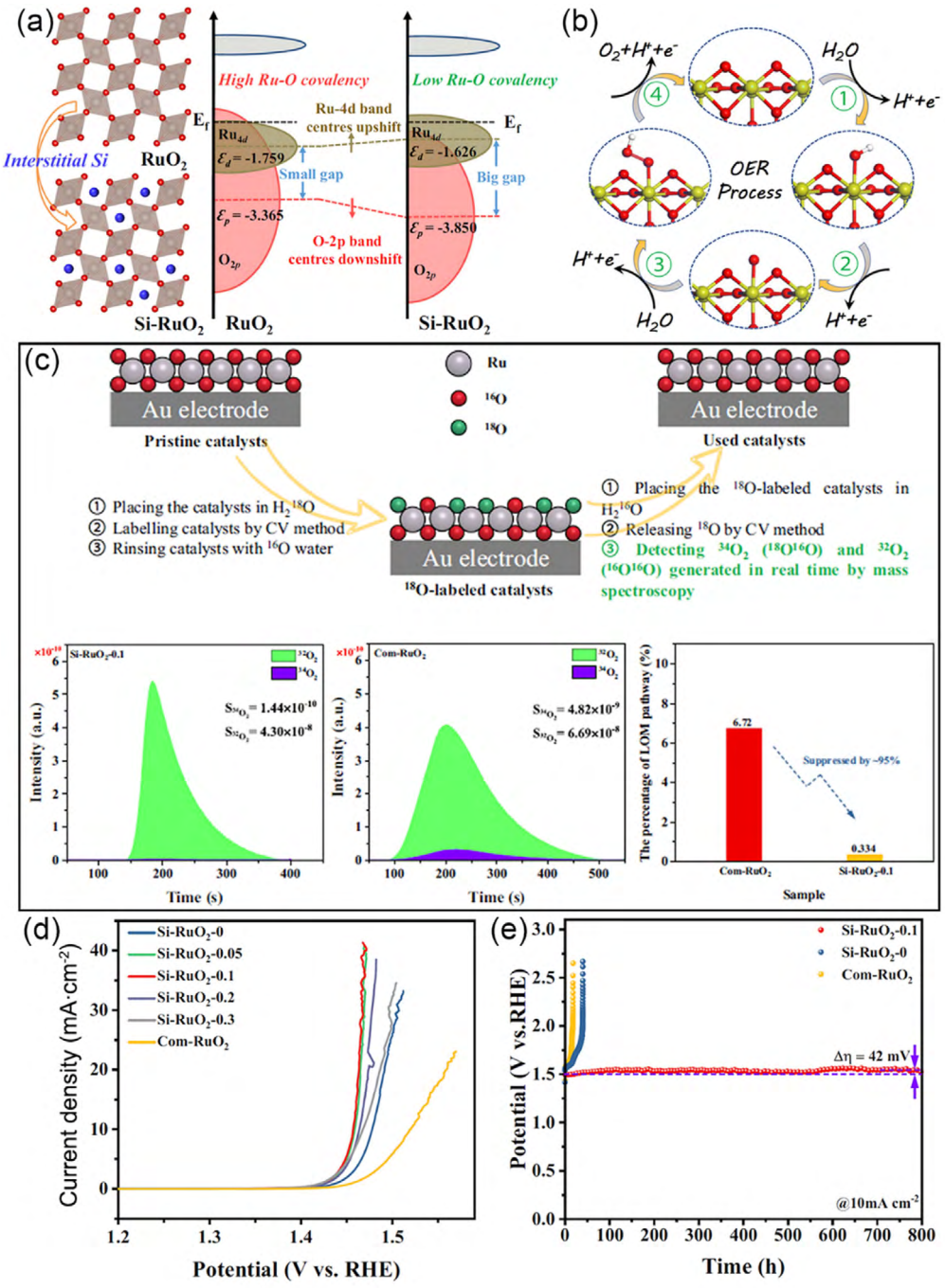


Fig. 8. (a) Crystal structures of RuO_2 (top) and Si-RuO_2 (bottom), and their corresponding band structures of Ru and O. (b) The four electrons mechanism of OER in an acidic solution. (c) DEMS signals of $^{34}O_2$ ($^{16}O^{18}O$) and $^{32}O_2$ ($^{16}O^{16}O$) from the produced oxygen gas for the ^{18}O-labeled Si-RuO_2-0.1 (b) and Com-RuO_2 (c) catalysts in 0.1 mol·L^{-1} $HClO_4$ electrolyte containing $H_2{}^{16}O$ as well as the percentage of O_2 gas through the LOM pathway in the OER. (d) LSV curves of Si-RuO_2 and Com-RuO_2 (with a loading of 0.30 mg_{cat}·cm^{-2}). (e) Chronopotentiometric stability curves of Si-RuO_2-0.1 and the control samples at 10 mA·cm^{-2}. Reproduced with permission [68].

[48]. The $NiCo_2(SOH)_x$ catalysts combine metal hydroxides' stability and metal chalcogenides' activity, resulting in higher OER activity and stability than mono-ligand catalysts and commercial precious metal ruthenium oxides. Firstly, the dual-ligand strategy can transfer electrocatalysts' magnetic structure to an antiferromagnetic state. After doping S into $Co(OH)_2$, the magnetic structure of $Co_3(SOH)_x$ becomes an antiferromagnetic state (Fig. 9b). It eliminates the paramagnetism of catalysts, weakening

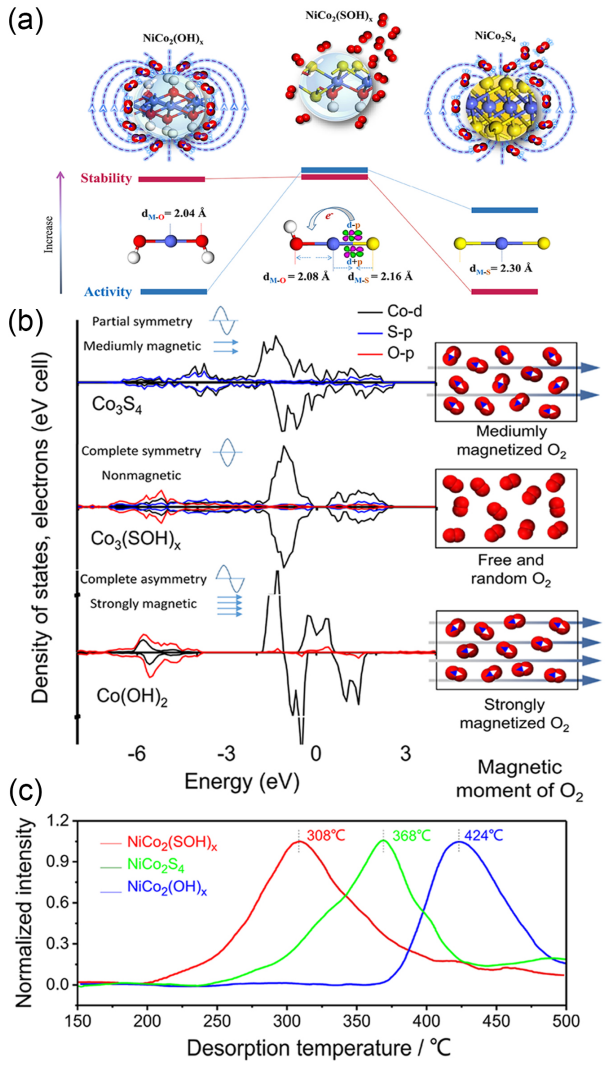


Fig. 9. (a) Schematic diagram of modulating the magnetic structure by dual-ligand synergistic modulation strategies; (b) calculated PDOS diagrams for $Co(OH)_2$, $Co_3(SOH)_x$, and Co_3S_4; (c) Temperature programmed desorption (TPD) plots of O atoms adsorbed on $NiCo_2(OH)_x$, $NiCo_2(SOH)_x$, and $NiCo_2S_4$. Reproduced with permission [48].

the adsorption strength of the O_2 product with paramagnetism and facilitating the release of active sites (Fig. 9c) [48]. In addition, the dual ligands of OH and S lead to the transfer of electrons from the M-S anti-bonding orbital to the M–O anti-bonding orbital (Fig. 10a). This electron transfer relatively weakens the super-strong M–O bonding while significantly strengthening the M–S bonding, achieving much-improved stability (Fig. 10b, 10c). At the same time, the transfer optimizes the binding energy of key intermediates (OH*, O*, and OOH*, Fig. 10d) [48]. DFT calculation revealed that the elaborately designed S and OH dual-ligand $NiCo_2(SOH)_x$ catalyst lowered the potential determined step of the OER from 0.7 eV for the mono-ligand catalysts to 0.3 eV for the dual-ligand catalysts (Fig. 10d). The $NiCo_2(SOH)_x$ exhibited an excellent OER activity with a very small overpotential of 0.29 V at a current density of 10 mA·cm^{-2} in Fig. 6f and a strong durability even after 30-hour accelerated ageing at a large current density of 100 mA·cm^{-2} (Fig. 10e) [48].

The effectiveness of the dual-ligand synergistic modulation strategy is further demonstrated with other anions like carbon and phosphorus. In C-Ni_3S_2, carbon doping reduces charge transfer from nickel to oxygen atoms, thereby weakening OH* and OOH* adsorption. This modification yields superior theoretical OER activity among X-Ni_3S_2 (X = C, P, N, O) systems, achieving the lowest theoretical overpotential (0.46 eV) [46]. Similarly, metal-organic framework (MOF)-derived porous Ni-Co-Fe ternary phosphide nanobricks (Ni-Co-Fe-P NBs) exhibit exceptional OER performance in 1.0 mol·L^{-1} KOH. DFT calculations confirm that coordinated Ni/Fe/P incorporation promotes the formation of catalytically active Co^{4+} sites while stabilizing oxygen-containing intermediates (OH*, O*, OOH*). The optimized Ni-Co-Fe-P NBs required remarkably low overpotentials of 187, 221, and 262 mV to achieve current densities of 10, 100, and 800 mA·cm^{-2}, respectively, coupled with an ultralow Tafel slope of 29 mV·dec^{-1} [28].

5. Conclusions and Perspectives

This review summarizes the achievements contributed by Professor Wei's group in efforts towards enhancing alkaline water electrolyzers' activity and stability. Through a series of comprehensive mechanistic studies for HER and OER processes, the team has identified key performance descriptors and developed feasible strategies focusing on optimizing the selective adsorption of critical intermediates, balancing the competing adsorption and desorption of multiple intermediates, enhancing the enrichment of activation species, modulating the surface orbital states of catalysts, and strengthening the coupling of intrinsic activity and mass transfer. Central to their discoveries is the recognition that metal/compound interfaces generate unique effects, particularly, the "chimney effect" and "local electric field enhancement", which dramatically improve HER performance under industrial operating conditions. For OER, the group has developed transformative strategies, including dual-ligand synergistic modulation, lattice oxygen suppression, and self-terminating surface reconstruction, all achieving simultaneous improvements in both activity and stability. Notably, the resulting catalysts surpass commercial benchmarks, demonstrating lower overpotentials than both Pt/C for HER and RuO_2 for OER at industrially relevant current densities.

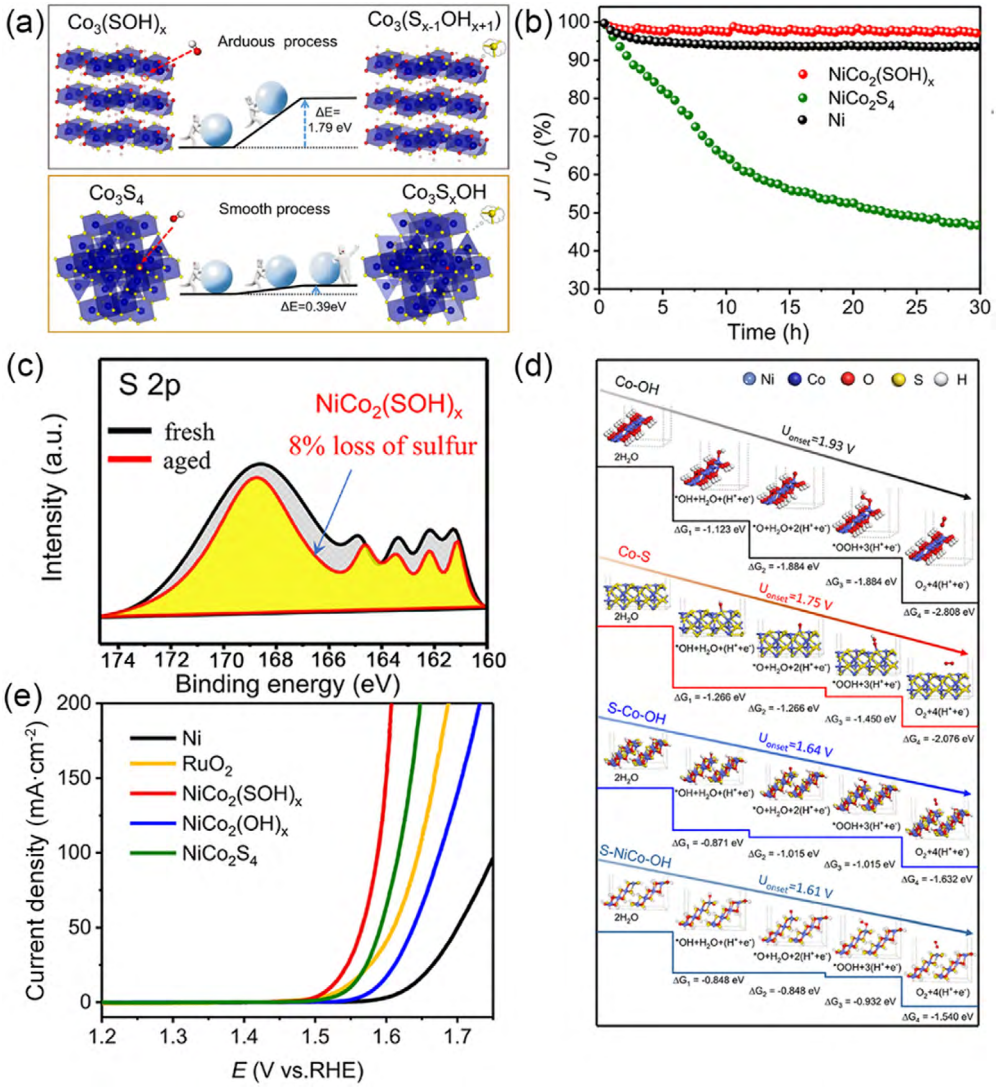


Fig. 10. (a) Total energy changes during the desulfuration processes of S^{2-} in Co_3S_4 (upper) and $Co_3(SOH)_x$ (bottom) replaced by OH^-; (b) Chronoamperometric curves of Ni, $NiCo_2(SOH)_x$ and $NiCo_2S_4$ at a current density of 100 mA·cm^{-2}; (c) the corresponded high-resolution S 2p XPS spectra of $NiCo_2(SOH)_x$ before and after ageing; (d) Reaction steps and corresponding free energy diagrams of the OER process on the pristine $Co(OH)_2$, $Co_3(SOH)_x$, $NiCo_2(SOH)_x$, and Co_3S_4; (e) LSV curves of Ni, $NiCo_2(SOH)_x$ and $NiCo_2S_4$. Reproduced with permission [48].

Nevertheless, sustaining HER/OER electrode activity in industrial alkaline water electrolyzers remains challenging. Reducing the gap between laboratory research and practical implementation demands continued efforts to design high-performance HER/OER electrodes, to understand reaction and deactivation mechanisms, and to develop new stability testing strategies. Here are some suggestions:

1) Developing novel strategies to enhance both activity and stability in electrocatalysts remains a critical priority. Current methods for improving electrode activity, such as doping, creating defects, increasing the exposure of active sites, and enlarging the electrochemically active surface area, often undermine stability. Issues like dopant leaching, oxygen vacancy filling, and nanomorphology destruction are significant drawbacks. Therefore, there is a pressing need for new strategies that can achieve simultaneous improvements in both activity and stability. The strategy of constructing metal/oxide interface introduced in this work significantly boosts activity without compromising stability. However, the level of activity enhancement directly depends on the density of these metal/oxide interfaces. Thus, it is essential to increase the interface density to maximize the catalytic activity of these materials.

2) Strengthening the adhesion between electrocatalysts and current collectors demands focused attention in ongoing research. The current densities in industrialised AWE can reach up to 500 mA·cm^{-2}. At

such a high current density, the abundant gas bubbles generated on the surface of the electrocatalyst can cause intense scouring, leading to the detachment of the electrocatalyst from the current collector. Currently, many reported electrocatalysts have high electrochemically active surface areas, which makes them prone to peeling off from the current collectors and ultimately leads to electrocatalyst deactivation. Therefore, enhancing the bonding strength between electrocatalysts and current collectors is a critical focus for future research. Several potential methods can create a strong bond with current collectors, such as electrodeposition, physical or chemical vapour deposition, and hot-dip coating. However, further investigation is still required for strategies that can produce large-area, highly active, and long-term electrodes at the lowest cost.

3) Intensifying research on electrocatalyst stability to meet industrial operating needs increased efforts. Currently, the evaluation of AWE electrocatalysts is mostly conducted using a three-electrode system under mild conditions, specifically, at temperatures of 25–30 °C and with an alkaline electrolyte concentration of 1 mol·L^{-1}. However, industrialised AWE typically operates under high-temperature (85 ~ 95 °C) and high-concentration (7 mol·L^{-1}) alkaline environments because it can enhance ionic conductivity, reduce solution resistance, and lower cell voltage, thus improving energy conversion efficiency. Unfortunately, the high temperatures and strong alkaline conditions accelerate the corrosion of electrocatalysts, promote the dissolution of active sites, and ultimately degrade stability. Therefore, the stability data obtained from traditional mild three-electrode systems cannot be directly applied to industrial-scale AWE. An in-depth investigation of the long-term stability of currently developed electrocatalysts under high-temperature, strong-alkaline conditions is urgently required.

4) Enhancing the chemical stability of electrocatalysts under high potentials constitutes a fundamental requirement for industrial deployment. In addition to high temperatures and strong alkalinity, the elevated potentials during industrial operations can alter the chemical state of catalysts, leading to deactivation. The cell voltage in industrial AWE typically ranges from 1.8 to 2.0 V. At this voltage range, the working potential of the cathode catalyst is generally below –0.1 V *vs.* RHE, while the anode potential often exceeds 1.8 V *vs.* RHE. Under such high potentials, electrocatalysts can be transformed into lower-activity compounds. For example, $Ni(OH)_2$ in $Ni/Ni(OH)_2$ electrocatalysts can easily be reduced to metallic Ni during HER, since the electrode potential for the $Ni(OH)_2/Ni$ pair is 0.1088 V *vs.* RHE. Similarly, in NiFe-Layered Double Hydroxide (LDH) electrocatalysts, iron can be readily oxidised to ferrate ions (FeO_4^{2-}), given that the electrode potential for $FeO_4^{2-}/Fe(OH)_3$ pair is 1.5488 V *vs.* RHE. Therefore, maintaining the stability of the electrocatalyst's chemical state under high potentials is a key strategy for enhancing its overall activity and longevity. The Quantum Well Catalytic Structure (QWCS) recently proposed by the authors, offers a novel approach to tackling this challenge.

5) Establishing rapid evaluation strategies for electrocatalyst stability represents an urgent need. Industrial AWE electrocatalysts must maintain a cell voltage increase of less than 10% over 10 years of continuous operation. While laboratory methods like galvanostatic testing and cyclic voltammetry effectively assess initial catalyst activity, validating decade-long stability through real-time operation remains impractical due to prohibitive time and cost constraints. Consequently, establishing a systematic, accelerated stability assessment strategy is critically needed to expedite the development of highly active, long-lived catalysts.

Conflicts of interest

The authors declare that they have no conflict of interest.

Acknowledgements

Authors acknowledge the financial supports from the National Key R&D Program of China (2021YFB4000300), National Natural Science Foundation of China (21822803, 22408030, 22072009, 91534205, 51072239), and National Program on Key Basic Research Project (973 Program, 2012CB720303).

Author contributions

Doctor Ling Zhang and Professor Li Li collaborated on this review. Wang-Yang Wu, Qiu-Yue Hu, and Shi-Dan Yang assisted in gathering and curating the literature. Professor Rui-Jin Liao offered crucial policy guidance for this review. As the Principal Investigator responsible for funding, Professor Zi-Dong Wei was instrumental in this project by proposing the review's core conceptual framework, overseeing the research design, and providing strategic policy support throughout the process.

Data availability

This study did not generate any new datasets. All data analyzed are from publicly available sources, as cited in the manuscript.

References

[1] [1] Barreto L, Makihira A, Riahi K. The hydrogen economy in the 21st century: A sustainable development scenario[J]. Int. J. Hydrogen Energy, 2003, 28(3): 267–284. https://doi.org/10.1016/S0360-3199(02)00074-5.

[2] Crabtree G W, Dresselhaus M S, Buchanan M V. The hydrogen economy[J]. Phy. Today, 2004, 57(12): 39–44. https://doi.org/10.1063/1.1878333.

[3] Penner S S. Steps toward the hydrogen economy[J]. Energy, 2006, 31(1): 33–43. https://doi.org/10.1016/j.energy.2004.04.060.

[4] Marbán G, Valdés-Solís T. Towards the hydrogen economy?[J]. Int. J. Hydrogen Energy, 2007, 32(12): 1625–1637. https://doi.org/10.1016/j.ijhydene.2006.12.017.

[5] Cook T R, Dogutan D K, Reece S Y, Surendranath Y, Teets T S, Nocera D G. Solar energy supply and storage for the legacy and nonlegacy worlds[J]. Chem. Rev., 2010, 110(11): 6474–6502. https://doi.org/10.1021/cr100246c.

[6] Walter M G, Warren E L, Mckone J R, Boettcher S W, Mi Q, Santori E A, Lewis N S. Solar water splitting cells[J]. Chem. Rev., 2010, 110(11): 6446–6473. https://doi.org/10.1021/cr1002326.

[7] Bockris J O M. The hydrogen economy: Its history[J]. Int. J. Hydrogen Energy, 2013, 38(6): 2579–2588. https://doi.org/10.1016/j.ijhydene.2012.12.026.

[8] Zeng Y, Zhao M T, Zeng H L, Jiang Q, Ming F W, Xi K, Wang Z C, Liang H F. Recent progress in advanced catalysts for electrocatalytic hydrogenation of organics in aqueous conditions[J]. eScience, 2023, 3(5): 100156–100178. https://doi.org/10.1016/j.esci.2023.100156.

[9] Chen M, Kitiphatpiboon N, Feng C, Abudula A, Ma Y F, Guan G Q. Recent progress in transition-metal-oxide-based electrocatalysts for the oxygen evolution reaction in natural seawater splitting: A critical review[J]. eScience, 2023, 3(2): 100111–100127. https://doi.org/10.1016/j.esci.2023.100111.

[10] Wang N, Song S Z, Wu W T, Deng Z F, Tang C. Bridging laboratory electrocatalysts with industrially relevant alkaline water electrolyzers[J]. Adv. Energy Mater., 2024, 14(16): 2303451–2303464. https://doi.org/10.1002/aenm.202303451.

[11] Man I C, Su H Y, Calle-Vallejo F, Hansen H A, Martínez J I, Inoglu N G, Kitchin J, Jaramillo T F, Nørskov J K, Rossmeisl J. Universality in oxygen evolution electrocatalysis on oxide surfaces[J]. ChemCatChem, 2011, 3(7): 1159–1165. https://doi.org/10.1002/cctc.201000397.

[12] Yang B L, Xiang Z H. Nanostructure engineering of cathode layers in proton exchange membrane fuel cells: From catalysts to membrane electrode assembly[J]. ACS Nano, 2024, 18(18): 11598–11630. https://doi.org/10.1021/acsnano.4c01113.

[13] Cao J F, Ji Y X, Shao Z Q. Nanotechnologies in ceramic electrochemical cells[J]. Chem. Soc. Rev., 2024, 53(1): 450–501. https://doi.org/10.1039/d3cs00303e.

[14] Ehlers J C, Feidenhans'l A A, Therkildsen K T, Larrazábal G O. Affordable green hydrogen from alkaline water electrolysis: Key research needs from an industrial perspective[J]. ACS Energy Lett., 2023, 8(3): 1502–1509. https://doi.org/10.1021/acsenergylett.2c02897.

[15] Zheng X Q, Zhang L, Huang J W, Peng L S, Deng M M, Li L, Li J, Chen H M, Wei Z D. Boosting Hydrogen evolution reaction of nickel sulfides by introducing nonmetallic dopants[J]. J. Phys. Chem. C, 2020, 124(44): 24223–24231. https://doi.org/10.1021/acs.jpcc.0c06971.

[16] Zhang L, Li L, Chen H M, Wei Z D. Recent progress in precious metal-free carbon-based materials towards the oxygen reduction reaction: Activity, stability, and anti-poisoning[J]. Chem. - Eur. J., 2020, 26(18): 3973–3990. https://doi.org/10.1002/chem.201904233.

[17] Zheng X, Li L, Wei Z D. Constructing and regulating electrocatalysts: from perspective of mesoscale[J]. CIESC Journal, 2020, 71(10): 4445–4461. https://doi.org/10.11949/0438-1157.202007.

[18] Zhang L, Cheng H M, Wei Z D. Recent advance in transition metal oxide-based materials for oxygen evolution reaction electrocatalysts[J]. CIESC J., 2020, 71(9): 3876–3904. https://doi.org/10.11949/0438-1157.20200573.

[19] Zhang L, Wang X Y, Zheng X Q, Peng L S, Shen J J, Xiang R, Deng Z H, Li L, Chen H M, Wei Z D. Oxygen-incorporated $NiMoP_2$ nanowire arrays for enhanced hydrogen evolution activity in alkaline solution[J]. ACS Appl. Energy Mater., 2018, 1(10): 5482–5489. https://doi.org/10.1021/acsaem.8b01044.

[20] Huang M H, Cao C S, Liu L, Wei W B, Zhu Q L, Huang Z G. Controlled synthesis of MOF-derived hollow and yolk-shell nanocages for improved water oxidation and selective ethylene glycol reformation[J]. eScience, 2023, 3(5): 100118–100126. https://doi.org/10.1016/j.esci.2023.100118.

[21] Liu K K, Meng Z, Fang Y, Jiang H L. Conductive MOFs for electrocatalysis and electrochemical sensor[J]. eScience, 2023, 3(6): 100133–100146. https://doi.org/10.1016/j.esci.2023.100133.

[22] Menezes P W, Walter C, Hausmann J N, Beltran-Suito R, Schlesiger C, Praetz S, Yu Verchenko V, Shevelkov A V, Driess M. Boosting water oxidation through in situ electroconversion of manganese gallide: An intermetallic precursor approach[J]. Angew. Chem. Int. Ed., 2019, 58(46): 16569–16574. https://doi.org/10.1002/anie.201909904.

[23] Zhang Z C, Liu G G, Cui X Y, Chen B, Zhu Y H, Gong Y, Saleem F, Xi S B, Du Y H, Borgna A, Lai Z C, Zhang Q H, Li B, Zong Y, Han Y, Gu L, Zhang H. Crystal phase and architecture engineering of lotus-thalamus-shaped Pt-Ni anisotropic superstructures for highly efficient electrochemical hydrogen evolution[J]. Adv. Mater., 2018, 30(30): e1801741. https://doi.org/10.1002/adma.201801741.

[24] Luo F, Zhang Q, Yu X X, Xiao S L, Ling Y, Hu H, Guo L, Yang Z H, Huang L, Cai W W, Cheng H S. Palladium phosphide as a stable and efficient electrocatalyst for overall water splitting[J]. Angew. Chem. Int. Ed., 2018, 57(45): 14862–14867. https://doi.org/10.1002/anie.201810102.

[25] Xu G R, Bai J, Jiang J X, Lee J M, Chen Y. Polyethyleneimine functionalized platinum superstructures: Enhancing hydrogen evolution performance by morphological and interfacial control[J]. Chem. Sci., 2017, 8(12): 8411–8418. https://doi.org/10.1039/c7sc04109h.

[26] Zhang L, Xiong K, Nie Y, Wang X X, Liao J H, Wei Z D. Sputtering nickel-molybdenum nanorods as an excellent hydrogen evolution reaction catalyst[J]. J. Power Sources, 2015, 297: 413–418. https://doi.org/10.1016/j.jpowsour.2015.08.004.

[27] Hu L, Yang B Z, Hou Z P, Lu Y F, Su W T, Li L W. Unlocking the charge doping effect in softly intercalated ultrathin ferromagnetic superlattice[J]. eScience, 2023, 3(3): 100117. https://doi.org/10.1016/j.esci.2023.100117.

[28] Li A, Zhang L, Wang F Z, Zhang L, Li L, Chen H M, Wei Z D. Rational design of porous Ni-Co-Fe ternary metal phosphides nanobricks as bifunctional electrocatalysts for efficient overall water splitting[J]. Appl. Catal. B, 2022, 310: 121353–121362. https://doi.org/10.1016/j.apcatb.2022.121353.

[29] Zhang L, Huang J W, Zheng Q Z, Li A, Li X L, Li J, Shao M H, Chen H M, Wei Z D, Deng Z H. "Superaerophobic" NiCo bimetallic phosphides for highly efficient hydrogen evolution reaction electrocatalysts[J]. Chem. Commun., 2021, 57(50): 6173–6176. https://doi.org/10.1039/D1CC01698A.

[30] Tong C, Xiang R, Peng L S, Tan L Q, Tang X Y, Wang J C, Li L, Liao Q, Wei Z D. Amorphous FeO_x (x = 1, 1.5) coated Cu3P nanosheets with bamboo leaves-like morphology induced by solvent molecule adsorption for highly active HER catalysts[J]. J. Mater. Chem. A, 2020, 8(6): 3351–3356. https://doi.org/10.1039/c9ta11779b.

[31] Peng L S, Liao M S, Zheng X Q, Nie Y, Zhang L, Wang M J, Xiang R, Wang J, Li L, Wei Z D. Accelerated alkaline hydrogen evolution on $M(OH)_x$/M-$MoPO_x$ (M = Ni, Co, Fe, Mn) electrocatalysts by coupling water dissociation and hydrogen ad-desorption steps[J]. Chem. Sci., 2020, 11(9): 2487–2493. https://doi.org/10.1039/c9sc04603h.

[32] Xiang R, Duan Y J, Tong C, Peng L S, Wang J, Shah S S A, Najam T, Huang X, Wei Z D. Self-standing FeCo Prussian blue analogue derived FeCo/C and FeCoP/C nanosheet arrays for cost-effective electrocatalytic water splitting[J].

Electrochim. Acta, 2019, 302: 45–55. https://doi.org/10.1016/j.electacta.2019.01.170.

[33] Cheng C, Shah S S A, Najam T, Zhang L, Qi X Q, Wei Z D. Highly active electrocatalysis of hydrogen evolution reaction in alkaline medium by Ni-P alloy: A capacitance-activity relationship[J]. J. Energy Chem., 2017, 26(6): 1245–1251. https://doi.org/10.1016/j.jechem.2017.09.028.

[34] Wang X, Yu M H, Feng X L. Electronic structure regulation of noble metal-free materials toward alkaline oxygen electrocatalysis[J]. eScience, 2023, 3(4): 100141–100160. https://doi.org/10.1016/j.esci.2023.100141.

[35] Anjum M a R, Lee M H, Lee J S. Boron-and nitrogen-codoped molybdenum carbide nanoparticles imbedded in a BCN network as a bifunctional electrocatalyst for hydrogen and oxygen evolution reactions[J]. ACS Catal., 2018, 8(9): 8296–8305. https://doi.org/10.1021/acscatal.8b01794.

[36] Wu Y H, He H W. A novel Ni-S-W-C electrode for hydrogen evolution reaction in alkaline electrolyte[J]. Mater. Lett., 2017, 209: 532–534. https://doi.org/10.1016/j.matlet.2017.08.086.

[37] Peng L S, Shen J J, Zhang L, Wang Y, Xiang R, Li J, Li L, Wei Z D. Graphitized carbon-coated vanadium carbide nanoboscages modified by nickel with enhanced electrocatalytic activity for hydrogen evolution in both acid and alkaline solutions[J]. J. Mater. Chem. A, 2017, 5(44): 23028–23034. https://doi.org/10.1039/c7ta07275a.

[38] Xiong K, Li L, Zhang L, Ding W, Peng L S, Wang Y, Chen S G, Tan S Y, Wei Z D. Ni-doped Mo_2C nanowires supported on Ni foam as a binder-free electrode for enhancing the hydrogen evolution performance[J]. J. Mater. Chem. A, 2015, 3(5): 1863–1867. https://doi.org/10.1039/c4ta05686h.

[39] Jing S Y, Lu J J, Yu G T, Yin S B, Luo L, Zhang Z S, Ma Y F, Chen W, Shen P K. Carbon-encapsulated wox hybrids as efficient catalysts for hydrogen evolution[J]. Adv. Mater., 2018, 30(28): 1705979–1705986. https://doi.org/10.1002/adma.201705979.

[40] Najam T, Ahmad Shah S S, Ding W, Ling Z, Li L, Wei Z D. Electron penetration from metal core to metal species attached skin in nitrogen-doped core-shell catalyst for enhancing oxygen evolution reaction[J]. Electrochim. Acta, 2019, 327: 134939–134947. https://doi.org/10.1016/j.electacta.2019.134939.

[41] Wang Y, Chen L H, Mao Z X, Peng L S, Xiang R, Tang X Y, Deng J H, Wei Z D, Liao Q. Controlled synthesis of single cobalt atom catalysts via a facile one-pot pyrolysis for efficient oxygen reduction and hydrogen evolution reactions[J]. Sci. Bull., 2019, 64(15): 1095–1102. https://doi.org/10.1016/j.scib.2019.06.012.

[42] Yan H J, Xie Y, Wu A P, Cai Z C, Wang L, Tian C G, Zhang X M, Fu H G. Anion-modulated HER and OER activities of 3d Ni-V-based interstitial compound heterojunctions for high-efficiency and stable overall water splitting[J]. Adv. Mater., 2019, 31(23): e1901174. https://doi.org/10.1002/adma.201901174.

[43] Li Y B, Tan X, Chen S, Bo X, Ren H J, Smith S C, Zhao C. Processable surface modification of nickel-heteroatom (N, S) bridge sites for promoted alkaline hydrogen evolution[J]. Angew. Chem. Int. Ed., 2019, 58(2): 461–466. https://doi.org/10.1002/anie.201808629.

[44] Yan J Q, Kong L Q, Ji Y J, Li Y T, White J, Liu S Z, Han X P, Lee S T, Ma T Y. Air-stable phosphorus-doped molybdenum nitride for enhanced elctrocatalytic hydrogen evolution[J]. Commun. Chem., 2018, 1(1): 1–10. https://doi.org/10.1038/s42004-018-0097-9.

[45] Zhang Y Q, Ouyang B, Xu J, Jia G C, Chen S, Rawat R S, Fan H J. Rapid synthesis of cobalt nitride nanowires: Highly efficient and low-cost catalysts for oxygen evolution[J]. Angew. Chem. Int. Ed., 2016, 55(30): 8670–8674. https://doi.org/10.1002/anie.201604372.

[46] Zheng X Q, Zhang L, He W, Li L, Lu S. Heteroatom-doped nickel sulfide for efficient electrochemical oxygen evolution reaction[J]. Energies, 2023, 16(2): 881–895. https://doi.org/10.3390/en16020881.

[47] Wang M J, Zheng X Q, Song L L, Feng X, Liao Q, Li J, Li L, Wei Z D. Fe_3O_4/FeS_2 heterostructures enable efficient oxygen evolution reaction[J]. J. Mater. Chem. A, 2020, 8(28): 14145–14151. https://doi.org/10.1039/c9ta13775k.

[48] Peng L S, Wang J, Nie Y, Xiong K, Wang Y, Zhang L, Chen K, Ding W, Li L, Wei Z D. Dual-ligand synergistic modulation: a satisfactory strategy for simultaneously improving the activity and stability of oxygen evolution electrocatalysts[J]. ACS Catal., 2017, 7(12): 8184–8191. https://doi.org/10.1021/acscatal.7b01971.

[49] Panda C, Menezes P W, Yao S L, Schmidt J, Walter C, Hausmann J N, Driess M. Boosting electrocatalytic hydrogen evolution activity with a $NiPt_3$@NiS heteronanostructure evolved from a molecular nickel-platinum precursor[J]. J. Am. Chem. Soc., 2019, 141(34): 13306–13310. https://doi.org/10.1021/jacs.9b06530.

[50] Deng S J, Luo M, Ai C Z, Zhang Y, Liu B, Huang L, Jiang Z, Zhang Q H, Gu L, Lin S W, Wang X L, Yu L, Wen J G, Wang J A, Pan G X, Xia X H, Tu J P. Synergistic doping and intercalation: Realizing deep phase modulation on MoS_2 arrays for high-efficiency hydrogen evolution reaction[J]. Angew. Chem. Int. Ed., 2019, 58(45): 16289–16296. https://doi.org/10.1002/anie.201909698.

[51] Chinese Society of Electrochemistry. The top ten scientific questions in electrochemistry[J]. J. Electrochem., 2024, 30(1): 2024121. https://doi.org/10.61558/2993-074x.3444.

[52] Nørskov J K, Bligaard T, Logadottir A, Kitchin J R, Chen J G, Pandelov S, Stimming U. Trends in the exchange current for hydrogen evolution[J]. J. Electrochem. Soc., 2005, 152(3): J23–J26. https://doi.org/10.1149/1.1856988.

[53] Hinnemann B, Moses P G, Bonde J, Joergensen K P, Nielsen J H, Horch S, Chorkendorff I, Noerskov J K. Biomimetic hydrogen evolution: MoS_2 nanoparticles as catalyst for hydrogen evolution[J]. J. Am. Chem. Soc., 2005, 36(25): 5308–5309. https://doi.org/10.1021/ja0504690.

[54] Zhang L, Huang J W, Zheng Q Z, Li A, Li X L, Li J, Shao M H, Chen H M, Wei Z D, Deng Z H, Li C. "Superaerophobic" NiCo bimetallic phosphides for highly efficient hydrogen evolution reaction electrocatalysts[J]. Chem. Commun., 2021, 57(50): 6173–6176. https://doi.org/10.1039/d1cc01698a.

[55] Angulo A, Van Der Linde P, Gardeniers H, Modestino M, Fernández Rivas D. Influence of bubbles on the energy conversion efficiency of electrochemical reactors[J]. Joule, 2020, 4(3): 555–579. https://doi.org/10.1016/j.joule.2020.01.005.

[56] Jia B B, Zhang B H, Cai Z, Yang X Y, Li L D, Guo L. Construction of amorphous/crystalline heterointerfaces for enhanced electrochemical processes[J]. eScience, 2023, 3(2): 100112. https://doi.org/10.1016/j.esci.2023.100112.

[57] Jiang J X, Liao J H, Tao S C, Najam T, Ding W, Wang H J, Wei Z D. Modulation of iridium-based catalyst by a trace of transition metals for hydrogen oxidation/evolution reaction in alkaline[J]. Electrochim. Acta, 2020, 333: 135444–135451. https://doi.org/10.1016/j.electacta.2019.135444.

[58] Xiong K, Li L, Deng Z H, Xia M R, Chen S G, Tan S Y, Peng X J, Duan C Y, Wei Z D. RuO_2 loaded into porous Ni as a synergistic catalyst for hydrogen production[J]. RSC Adv., 2014, 4(39): 20521–20526. https://doi.org/10.1039/c4ra01379d.

[59] Meng Z Y, Qiu Z M, Shi Y X, Wang S X, Zhang G X, Pi Y C, Pang H. Micro/nano metal-organic frameworks meet energy chemistry: A review of materials synthesis and applications[J]. eScience, 2023, 3(2): 100092. https://doi.org/https://doi.org/10.1016/j.esci.2023.100092.

[60] Trasatti S. Work function, electronegativity, and electrochemical behaviour of metals: III. Electrolytic hydrogen evolution in acid solutions[J]. J. Electroanal. Chem., 1972, 39(1): 163–184. https://doi.org/10.1016/S0022-0728(72)80485-6.

[61] Peng L S, Zheng X Q, Li L, Zhang L, Yang N, Xiong K, Chen H M, Li J, Wei Z D. Chimney effect of the interface in metal oxide/metal composite catalysts on the hydrogen evolution reaction[J]. Appl. Catal. B, 2019, 245: 122–129. https://doi.org/10.1016/j.apcatb.2018.12.035.

[62] Subbaraman R, Tripkovic D, Chang K C, Strmcnik D, Paulikas A P, Hirunsit P, Chan M, Greeley J, Stamenkovic V, Markovic N M. Trends in activity for the water electrolyser reactions on 3d M(Ni,Co,Fe,Mn) hydr(oxy)oxide catalysts[J]. Nat. Mater., 2012, 11(6): 550–557. https://doi.org/10.1038/nmat3313.

[63] Subbaraman R, Tripkovic D, Strmcnik D, Chang K-C, Uchimura M, Paulikas A P, Stamenkovic V, Markovic N M. Enhancing hydrogen evolution activity in water splitting by tailoring Li^+-$Ni(OH)_2$-Pt interfaces[J]. Science, 2011, 334(6060): 1256–1260. https://doi.org/10.1126/science.1211934.

[64] Rossmeisl J, Logadottir A, Nørskov J K. Electrolysis of water on (oxidized) metal surfaces[J]. Chem. Phys., 2005, 319(1-3): 178–184. https://doi.org/10.1016/j.chemphys.2005.05.038.

[65] Rossmeisl J, Qu Z W, Zhu H, Kroes G J, Nørskov J K. Electrolysis of water on oxide surfaces[J]. J. Electroanal. Chem., 2007, 607(1-2): 83–89. https://doi.org/10.1016/j.jelechem.2006.11.008.

[66] Yoo J S, Rong X, Liu Y, Kolpak A M. Role of lattice oxygen participation in understanding trends in the oxygen evolution reaction on perovskites[J]. ACS Catal., 2018, 8(5): 4628–4636. https://doi.org/10.1021/acscatal.8b00612.

[67] Grimaud A, Diaz-Morales O, Han B, Hong W T, Lee Y L, Giordano L, Stoerzinger K A, Koper M T M, Shao-Horn Y. Activating lattice oxygen redox reactions in metal oxides to catalyse oxygen evolution[J]. Nat. Chem., 2017, 9(5): 457–465. https://doi.org/10.1038/nchem.2695.

[68] Ping X Y, Liu Y D, Zheng L X, Song Y, Guo L, Chen S G, Wei Z D. Locking the lattice oxygen in RuO_2 to stabilize highly active Ru sites in acidic water oxidation[J]. Nat. Commun., 2024, 15(1): 2501–2511. https://doi.org/10.1038/s41467-024-46815-6.

[69] Chang J W, Shi Y Y, Wu H, Yu J K, Jing W, Wang S Y, Waterhouse G I N, Tang Z Y, Lu S Y. Oxygen radical coupling on short-range ordered Ru atom arrays enables exceptional activity and stability for acidic water oxidation[J]. J. Am. Chem. Soc., 2024, 146(19): 12958–12968. https://doi.org/10.1021/jacs.3c13248.

[70] Kang W C, Wei R F, Yin H, Li D F, Chen Z, Huang Q G, Zhang P F, Jing H W, Wang X L, Li C. Unraveling sequential oxidation kinetics and determining roles of multi-cobalt active sites on Co_3O_4 catalyst for water oxidation[J]. J. Am. Chem. Soc., 2023, 145(6): 3470–3477. https://doi.org/10.1021/jacs.2c11508.

[71] Pushkar Y, Pineda-Galvan Y, Ravari A K, Otroshchenko T, Hartzler D A. Mechanism for O–O bond formation via radical coupling of metal and ligand based radicals: A new pathway[J]. J. Am. Chem. Soc., 2018, 140(42): 13538–13541. https://doi.org/10.1021/jacs.8b06836.

[72] Strmcnik D, Uchimura M, Wang C, Subbaraman R, Danilovic N, Van Der Vliet D, Paulikas A P, Stamenkovic V R, Markovic N M. Improving the hydrogen oxidation reaction rate by promotion of hydroxyl adsorption[J]. Nat. Chem., 2013, 5(4): 300–306. https://doi.org/10.1038/nchem.1574.

[73] Koper M T M. Thermodynamic theory of multi-electron transfer reactions: Implications for electrocatalysis[J]. J. Electroanal. Chem., 2011, 660(2): 254–260. https://doi.org/10.1016/j.jelechem.2010.10.004.

[74] Fabbri E, Nachtegaal M, Binninger T, Cheng X, Kim B J, Durst J, Bozza F, Graule T, Schaublin R, Wiles L, Pertoso M, Danilovic N, Ayers K E, Schmidt T J. Dynamic surface self-reconstruction is the key of highly active perovskite nano-electrocatalysts for water splitting[J]. Nat. Mater., 2017, 16(9): 925–931. https://doi.org/10.1038/nmat4938.

[75] Deng M M, Li M T, Jiang S K, Nie Y, Li L, Wei Z D. Interfacial water enrichment and reorientation on Pt/C catalysts induced by metal oxides participation for boosting the hydrogen evolution reaction[J]. J. Phys. Chem. Lett., 2022, 13(4): 1069–1076. https://doi.org/10.1021/acs.jpclett.1c03808.

[76] Boudart M, Vannice M A, Benson J E. Adlineation, portholes and spillover[J]. Zeitschrift für Physikalische Chemie, 1969, 64: 171–177. https://doi.org/10.1524/zpch.1969.64.1_4.171.

[77] Deng M M, Yang H M, Peng L S, Zhang L, Tan L Q, He G J, Shao M H, Li L, Wei Z D. Insight into the boosted activity of TiO_2-CoP composites for hydrogen evolution reaction: Accelerated mass transfer, optimized interfacial water, and promoted intrinsic activity[J]. J. Energy Chem., 2022, 74: 111–120. https://doi.org/10.1016/j.jechem.2022.06.047.

[78] Zheng X Q, Peng L S, Li L, Yang N, Yang Y, Li J, Wang J C, Wei Z D. Role of non-metallic atoms in enhancing the catalytic activity of nickel-based compounds for hydrogen evolution reaction[J]. Chem. Sci., 2018, 9(7): 1822–1830. https://doi.org/10.1039/c7sc04851c.

[79] Zhang L, Wang X Y, Li A, Zheng X Q, Peng L S, Huang J W, Deng Z H, Chen H M, Wei Z D. Rational construction of macroporous CoFeP triangular plate arrays from bimetal-organic frameworks as high-performance overall water-splitting catalysts[J]. J. Mater. Chem. A, 2019, 7(29): 17529–17535. https://doi.org/10.1039/c9ta05282h.

[80] Peng L S, Shen J J, Zheng X Q, Xiang R, Deng M M, Mao Z X, Feng Z P, Zhang L, Li L, Wei Z D. Rationally design of monometallic NiO-Ni_3S_2/NF heteronanosheets as bifunctional electrocatalysts for overall water splitting[J]. J. Catal., 2019, 369: 345–351. https://doi.org/10.1016/j.jcat.2018.11.023.

[81] Zheng X Q, Li L, Deng M M, Li J, Ding W, Nie Y, Wei Z D. Understanding the effect of interfacial interaction on metal/metal oxide electrocatalysts for hydrogen evolution and hydrogen oxidation reactions on the basis of first-principles calculations[J]. Catal. Sci. Technol., 2020, 10(14): 4743–4751. https://doi.org/10.1039/d0cy00960a.

[82] Li M T, Xie Z Y, Zheng X Q, Li L, Li J, Ding W, Wei Z D. Revealing the regulation mechanism of Ir-MoO_2 interfacial chemical bonding for improving hydrogen oxidation reaction[J]. ACS Catal., 2021, 11(24): 14932–14940. https://doi.org/10.1021/acscatal.1c04440.

[83] Seh Z W, Fredrickson K D, Anasori B, Kibsgaard J, Strickler A L, Lukatskaya M R, Gogotsi Y, Jaramillo T F, Vojvodic A. Two-dimensional molybdenum carbide (MXene) as an efficient electrocatalyst for hydrogen evolution[J]. ACS Energy Lett., 2016, 1(3): 589–594. https://doi.org/10.1021/acsenergylett.6b00247.

[84] Hammer B, Nørskov J K. Theoretical surface science and catalysis—calculations and concepts[J]. Adv. Catal., 2000, 45: 71–129. https://doi.org/10.1016/S0360-0564(02)45013-4.

[85] Liu Y, Liu S L, Wang Y, Zhang Q H, Gu L, Zhao S C, Xu D D, Li Y F, Bao J C, Dai Z H. Ru modulation effects in the synthesis of unique rod-like Ni@Ni_2P-Ru heterostructures and their remarkable electrocatalytic hydrogen evolution performance[J]. J. Am. Chem. Soc., 2018, 140(8): 2731–2734. https://doi.org/10.1021/jacs.7b12615.

[86] Wexler R B, Martirez J M P, Rappe A M. Chemical pressure-driven enhancement of the hydrogen evolving activity of Ni_2P from nonmetal surface doping interpreted via machine learning[J]. J. Am. Chem. Soc., 2018, 140(13): 4678–4683. https://doi.org/10.1021/jacs.8b00947.

[87] Caban-Acevedo M, Stone M L, Schmidt J R, Thomas J G, Ding Q, Chang H C, Tsai M L, He J H, Jin S. Efficient hydrogen evolution catalysis using ternary pyrite-type cobalt phosphosulphide[J]. Nat. Mater., 2015, 14(12): 1245–1251. https://doi.org/10.1038/nmat4410.

[88] Yao Y C, Hu S L, Chen W X, Huang Z Q, Wei W C, Yao T, Liu R R, Zang K T, Wang X Q, Wu G, Yuan W J, Yuan T W, Zhu B Q, Liu W, Li Z J, He D S, Xue Z G, Wang Y, Zheng X S, Dong J C, Chang C R, Chen Y X, Hong X, Luo J, Wei S Q, Li W X, Strasser P, Wu Y, Li Y D. Engineering the electronic structure of single atom Ru sites via compressive strain boosts acidic water oxidation electrocatalysis[J]. Nat. Catal., 2019, 2(4): 304–313. https://doi.org/10.1038/s41929-019-0246-2.

[89] Li L, Feng X H, Nie Y, Chen S G, Shi F, Xiong K, Ding W, Qi X, Hu J S, Wei Z D, Wan L J, Xia M R. Insight into the effect of oxygen vacancy concentration on the catalytic performance of MnO2[J]. ACS Catal., 2015, 5(8): 4825–4832. https://doi.org/10.1021/acscatal.5b00320.

[90] Xie X H, Song M A, Wang L G, Engelhard M H, Luo L L, Miller A, Zhang Y Y, Du L, Pan H L, Nie Z M, Chu Y Y, Estevez L, Wei Z D, Liu H, Wang C M, Li D S, Shao Y Y. Electrocatalytic hydrogen evolution in neutral pH solutions: Dual-phase synergy[J]. ACS Catal., 2019, 9(9): 8712–8718. https://doi.org/10.1021/acscatal.9b02609.

[91] Hu C Y, Ma Q Y, Hung S F, Chen Z N, Ou D H, Ren B, Chen H M, Fu G, Zheng N F. In situ electrochemical production of ultrathin nickel nanosheets for hydrogen evolution electrocatalysis[J]. Chem, 2017, 3(1): 122–133. https://doi.org/10.1016/j.chempr.2017.05.011.

[92] Speck F D, Dettelbach K E, Sherbo R S, Salvatore D A, Huang A, Berlinguette C P. On the electrolytic stability of iron-nickel oxides[J]. Chem, 2017, 2(4): 590–597. https://doi.org/10.1016/j.chempr.2017.03.006.

[93] Zhao J W, Zhang H, Li C F, Zhou X, Wu J Q, Zeng F, Zhang J W, Li G R. Key roles of surface Fe sites and Sr vacancies in the perovskite for an efficient oxygen evolution reaction via lattice oxygen oxidation[J]. Energy Environ. Sci., 2022, 15(9): 3912–3922. https://doi.org/10.1039/d2ee00264g.

[94] Song F, Bai L, Moysiadou A, Lee S, Hu C, Liardet L, Hu X. Transition metal oxides as electrocatalysts for the oxygen evolution reaction in alkaline solutions: An application-inspired renaissance[J]. J. Am. Chem. Soc., 2018, 140(25): 7748–7759. https://doi.org/10.1021/jacs.8b04546.

[95] Ma Q Y, Hu C Y, Liu K L, Hung S F, Ou D H, Chen H M, Fu G, Zheng N F. Identifying the electrocatalytic sites of nickel disulfide in alkaline hydrogen evolution reaction[J]. Nano Energy, 2017, 41: 148–153. https://doi.org/10.1016/j.nanoen.2017.09.036.

[96] Geiger S, Kasian O, Ledendecker M, Pizzutilo E, Mingers A M, Fu W T, Diaz-Morales O, Li Z, Oellers T, Fruchter L, Ludwig A, Mayrhofer K J J, Koper M T M, Cherevko S. The stability number as a metric for electrocatalyst stability benchmarking[J]. Nat. Catal., 2018, 1(7): 508–515. https://doi.org/10.1038/s41929-018-0085-6.

[97] Li A, Tang X X, Cao R J, Song D C, Wang F Z, Yan H, Chen H M, Wei Z D. Directed surface reconstruction of Fe modified Co_2VO_4 spinel oxides for water oxidation catalysts experiencing self-terminating surface deterioration[J]. Adv. Mater., 2024: 2401818–2401828. https://doi.org/10.1002/adma.202401818.

[98] Xiang R, Tong C, Wang Y, Peng L S, Nie Y, Li L, Huang X, Wei Z D. Hierarchical coral-like FeNi(OH)/Ni via mild corrosion of nickel as an integrated electrode for efficient overall water splitting[J]. Chin. J. Catal., 2018, 39(11): 1736–1745. https://doi.org/10.1016/s1872-2067(18)63150-x.

[99] Ahmad R, Kuppusamy P. Theory, instrumentation, and applications of electron paramagnetic resonance oximetry[J]. Chem. Rev., 2010, 110(5): 3212–3236. https://doi.org/10.1021/cr900396q.

系列综述 (2/4)：重庆大学魏子栋教授课题组在电化学能源转换方面的研究进展：高性能碱性电解水催化剂

张伶[a]，吴汪洋[a]，胡秋月[a]，杨世丹[a]，李莉[a,*]，廖瑞金[b]，魏子栋[a,*]
[a]特种化学电源全国重点实验室, 重庆大学化学化工学院, 重庆 40044
[b]输配电装备及系统安全与新技术国家重点实验室，重庆大学电气工程学院，重庆 40044

摘要：

大规模部署电解水制氢技术需要高性能的电催化剂。魏子栋教授课题组针对电解水制氢电极在工业工况条件下运行面临的关键科学与技术问题，持续致力于开展析氢/析氧催化反应机理解析，提升工况条件活性与稳定性的基础科学问题研究。本综述系统地总结了该课题组近十多年围绕高性能析氢和析氧电极研究所取得的进展。首先分析了电解水制氢面临着的析氢反应动力学速率缓慢与析氧反应活性/稳定性相互制约的原因，提出了调控电解水性能的“12345”原则。进而，针对碱水析氢催化剂，发现了复合相界面增强析氢活性的“烟囱效应”和“定域电场增强效应”，利用相界面调控，优化关键物种的选择性吸附、促进界面水分子富集-再定向与活化来强化高极化条件下的传质与反应，提升工业工况反应动力学。对析氧催化剂，提出了“双阴离子调控”、“晶格氧抑制”以及“表面自修复”等策略，通过平衡不同含氧物种吸附强度、调控磁性、增强金属-氧键强度和重组表面动态结构等实现活性与稳定性的同步提升。最后，本文总结了目前析氢/析氧催化剂在工业级碱水槽应用时面临的长周期活性和稳定性的挑战，并提出了未来的研究方向。

关键词：碱水电解制氢；析氢反应；析氧反应；活性；稳定性